An Assessment of Hypocenter Errors Associated with the Seismic Monitoring of Induced Hydro-fracturing in Hydrocarbon Reservoirs

Ellen S. Gilliland

Thesis submitted to the faculty of the Virginia Polytechnic Institute and State University in partial fulfillment of the requirements for the degree of

Master of Science
In
Geosciences

John A. Hole
Martin C. Chapman
Chester J. Weiss

October 14, 2009
Blacksburg, VA

Keywords: hydro-fracture treatment, hypocenter location error, hypocenter inversion algorithm, multi-well survey, velocity structure, arrival-time picking error, geometric constraint

An Assessment of Hypocenter Errors Associated with the Seismic Monitoring of Induced Hydro-fracturing in Hydrocarbon Reservoirs

Ellen S. Gilliland

ABSTRACT

Expanding the standard, single-well recording geometry used to monitor seismicity during hydro-fracture treatments could provide more accurate hypocenter locations and seismic velocities, improving general reservoir characterization. However, for the real, two-well data set obtained for this project, only S-wave picks were available, and testing resulted in anomalous hypocenter location behavior. This study uses a hypocenter location algorithm and both real and synthetic data sets to investigate how the accuracy of the velocity model, starting hypocenter location, recording geometry, and arrival-time picking error affect final hypocenter locations.

Hypocenter locations improved using a velocity model that closely matched the observed sonic log rather than a smoothed version of this model. The starting hypocenter location did not affect the final location solution if both starting and final locations were between the wells. Two solutions were possible when the true solution was not directly between the wells. Adding realistic random picking errors to synthetic data closely modeled the dispersed hypocenter error pattern observed in the real data results. Adding data from a third well to synthetic tests dramatically reduced location error and removed horizontal geometric bias observed in the two-well case.

Seismic event data recorded during hydro-fracture treatments could potentially be used for three-dimensional joint hypocenter-velocity tomography. This would require observation wells close enough to earthquakes to record P- and S-wave arrivals or wells at orientations sufficient to properly triangulate hypocenter locations. Simulating results with synthetic tests

before drilling could optimize survey design to collect data more effectively and make analysis more useful.

Acknowledgments

I would like to thank Pinnacle Technologies and BP for providing a real data set and processing software. Special thanks to Charlie Waltman and Sean Machovoe for their interest and involvement with this project.

Sincere thanks to my committee members, John, Martin, and Chet, for their thoughtful input and guidance throughout this project. I feel fortunate to have known each of you as teachers, mentors, and colleagues during my time at Virginia Tech and thank you for your contributions to my graduate school experience.

Sincere thanks also to Jake Beale, whose research help and encouragement have both been invaluable.

Thanks to the geosciences technical staff, especially Richard Godbee and Miles Gentry for helping with Fortran commands, far too many hard drive crashes, and countless other computing emergencies. Thanks also to the geosciences administrative staff, especially Connie Lowe, who in addition to many other things, has been a great friend.

Thanks to all my officemates in the 1070 cubicle farm and in the 1068-A geophysics annex. I can only hope my next office has such entertaining characters. I hope you continue the potlucks and wish you the best as you finish your degrees.

Heartfelt thanks to my wonderful parents, Alison and Kirby, who have always encouraged and enabled my academic goals. Your support, honest advice, and friendship help me thrive wherever I roam. Thanks to my brother, Lytton, whose creativity, intelligence, and kindness inspired me growing up and continue to now. Thanks to my Aunt Lynne and Uncle George, whose love of science and the natural world refreshes mine. Thanks to my Aunt Ann, a loyal fan who can share victories or raise spirits from across the country.

Very special thanks to all of my Blacksburg friends. New friendships have been the best part of my decision to attend Virginia Tech, and I leave glad to know that many of them will be lifelong.

Finally, thanks to Alan Witten, my first mentor in geophysics, who saw the potential in students of all ages and invested in one very grateful high school student many years ago.

Table of Contents

List of Figures

List of Tables

Introduction

Hydrocarbon materials reside within the pore space of sedimentary reservoir rocks. Their extraction is limited to the volume of pore space connected to the drill hole by permeability pathways. When connectivity and, therefore, extraction are prevented by the sealing of pores, drillers often choose to induce fracturing in the reservoir rock. In this process, called a "hydro-fracture treatment," a liquid or gel is pumped through an injection well into the reservoir at pressure sufficient to fracture the rock (Figure 1.1). A "proppant," a highly permeable sand or other solid, is sometimes combined with the liquid or gel to ensure that new fractures are held open, allowing enhanced production along new permeability pathways.

The mechanism by which fractures form is akin to the shear mechanism of an earthquake, and the micro-scale vibrations created by fracturing are essentially micro-earthquakes, with typical magnitudes ranging from -1 to -4. The microseismicity associated with the fracturing process can be monitored and recorded by receiver arrays placed down observation wells if the arrays are within the necessary proximity to detect the small events (~1500-2000 feet). First-arrival travel times from the resulting seismic records, combined with a one-dimensional seismic velocity model, can be used to locate the micro-earthquakes. The event locations disclose important information about the structure of the fracture network, connectivity within the reservoir (and potentially within surrounding geologic units), and the induced fracturing process itself.

In a typical induced fracturing survey, microseismic events are recorded on a vertical receiver array at a single, vertical observation well and are located using a one-dimensional velocity model. For this case, the depth of an event can be constrained by the difference in travel times to different receiver depths (Figure 1.2). The radial distance of an event from the well can

also be determined from the travel time. The azimuth of an event, however, cannot be constrained for the one-well case. The laterally-homogeneous, one-dimensional velocity model means that the location solution for an event at known coordinates (R, Z) is the same for all possible azimuths about the well. Hodograms are records of three-dimensional particle motion associated with seismic events. By indicating the direction for wave arrivals, hodograms can help narrow the range of possible event azimuths. However, even with the aid of hodogram analysis, error in the azimuthal direction remains large compared to that for depth and radial distance, reducing the overall quality of absolute event locations. This difficulty of resolving azimuth in the one-well case is well known (Rutledge, Phillips, and Mayerhofer, 2004).

The standard one-dimensional velocity model used to locate events is based on one-dimensional sonic log data. The model, therefore, is an assumption, as one-dimensional data cannot accurately represent lateral heterogeneities in velocity structure. In addition to possibly misrepresenting the true geology, a false velocity model can be detrimental to accurate event locations.

A survey in which microseismicity is recorded simultaneously at multiple observation well locations has potential to improve absolute event locations and can also improve the seismic velocity model beyond one dimension. A second observation well on the opposite side of an event cluster provides dense ray coverage in the crosswell region (Figure 1.3, (A)) and geometrical constraint on event azimuth (Figure 1.3 (B)). The addition of this second recording well could provide useful geologic and engineering data not possible with a standard, single-well recording geometry. This potential of the two-well case motivates this study.

This study uses a hypocenter location algorithm (Hole et al., 2000) and both real and synthetic data sets to investigate sources of location error in the two-well case. The real

microseismic data were recorded simultaneously on receiver arrays at two vertical observation wells during an induced fracture treatment of the Red Oak sandstone reservoir in the hydrocarbon-rich Arkoma Basin of southeast Oklahoma. The data were provided by Pinnacle Technologies, Inc. and BP p.l.c. Synthetic data mimicking the real data set were generated to control investigations of the source of the location error. The location algorithm uses a three-dimensional velocity model, initial hypocenter locations, receiver locations, and traveltime picks as input and employs a finite-difference traveltime algorithm to invert for new, updated hypocenter locations (Hole et al., 2000). Uncertainty on the input presents a liability for error in the inversion (e.g. Giardini, 1992, Phillips and Fehler, 1991). This study explores how the accuracy of the velocity model, starting hypocenters, two-well receiver geometry, and traveltime picks affects location quality. The objective is an improved understanding of the location error that exists in the real data set, as well as broader insights for predicting and assessing errors for other data sets. Such understanding can help optimize data collection and inversion to improve the accuracy of relocated hypocenters.

Figures

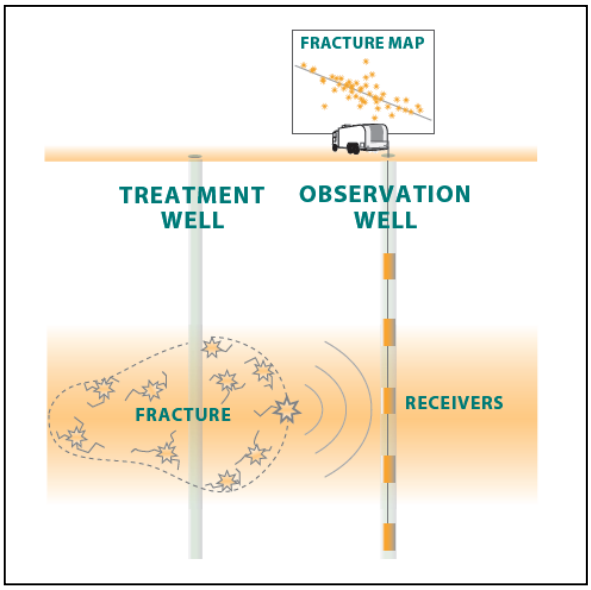

Figure 1.1: Schematic of induced hydro-fracture treatment (image used with permission of Pinnacle Technologies, Inc.).

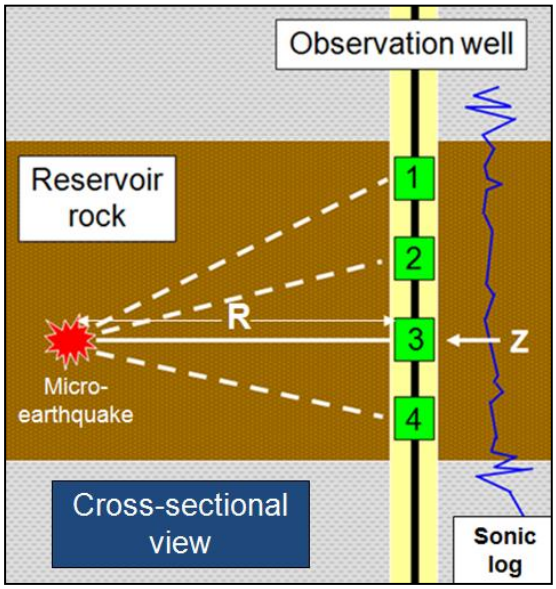

Figure 1.2: Hypocenter constraint with one observation well. Arrival time data at a vertical receiver array at depth (green boxes) can locate a micro-earthquake in depth (z) and radial distance (R), but cannot constrain the event azimuth with respect to the array.

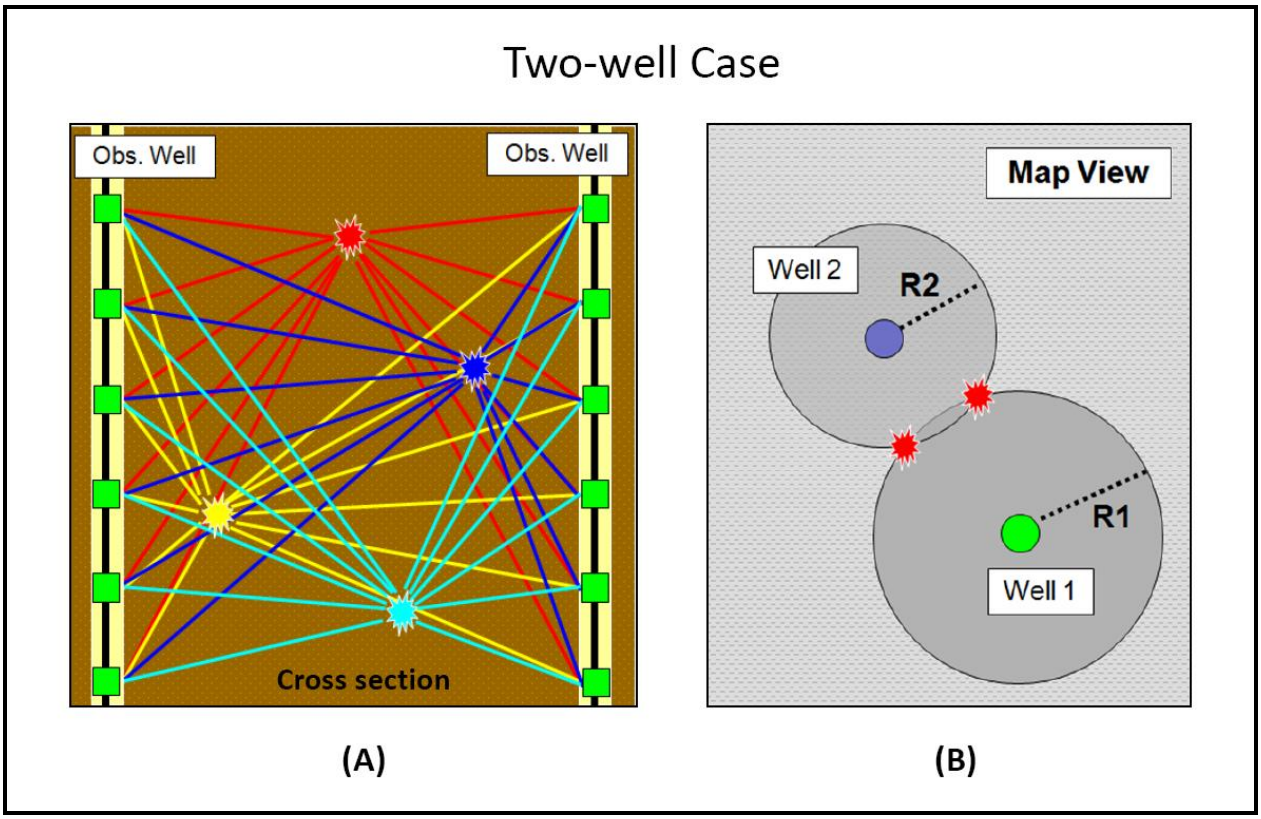

Figure 1.3: Improved hypocenter constraint with two observation wells. Adding a second observation well provides dense ray coverage in the crosswell region (A) and better constrains event location in the azimuthal direction (B). However, two event locations are still possible.

Geologic Setting

Continental collision and shortening causes localized mass accumulation, which, in turn, causes downward flexure of the lithosphere, forming foreland basins where eroded sediment collects (Figure 2.1) (DeCelles and Giles, 1996). The combination of rapidly deposited, orogen-derived sediments and active subsidence makes foreland basins prime settings for hydrocarbon generation (Schwab, 1985).

The Arkoma basin of southeast Oklahoma and west Arkansas (Figure 2.2) is a foreland basin formed in association with Ouachita-Marathon orogenesis during the middle Mississippian (Byrnes and Lawyer, 1999). During orogenesis, the proto-South American plate collided with the passive continental margin of the proto-North American plate. The resulting tectonism ultimately gave rise to the east-west trending Ouachita Mountains with the Arkoma basin forming syn-orogenically to the northwest. The Ouachitas eroded rapidly, filling the basin with a sequence of sandstones, containing highly economic hydrocarbon deposits (McGilvery and Houseknecht, 2000).

The Arkoma basin province spans over 30,000 square miles bounded by the Ozark Plateau to the north, the Choctaw and Ross Creek faults at its southern contact with the Ouachitas, the Arbuckle Mountains to the west, and the Mississippi embayment to the east (Figure 2.3) (Perry, 1995; Byrnes and Lawyer, 1999). Sedimentary rock thicknesses range from 3,000 to 20,000 feet within the basin and include many slope channel and marginal-submarine fan deposits (Perry, 1995; McGilvery and Houseknecht, 2000). The formation and entrapment of hydrocarbons within these sediments occurred during a relatively short period, from the start of Atokan time (~311 Mya) in the mid-Pennsylvanian to early Permian (~296 Mya) (Byrnes and

Lawyer, 1999). Hydrocarbon exploration and production in the basin has been successful and long-lasting and includes several major reservoirs (Boyd, 2005; Perry, 1995).

The Red Oak-Norris gas field is the largest in the Arkoma basin and the third largest in the state of Oklahoma (Figure 2.4) (Houseknecht and McGilvery, 1991; Boyd, 2005). Active since 1931, the field produces more than 150 million cubic feet per day and holds ultimate reserves exceeding 2 trillion cubic feet (Boyd, 2005; Houseknecht and McGilvery, 1991). The Atokan Spiro and Red Oak sandstones are major reservoirs, sourced by underlying shales and secured by a combination of stratigraphic and structural traps (Houseknecht and McGilvery, 1991; Perry, 1995).

The basal Atokan Spiro sandstone is a quartz arenite with a porosity of 11-15 percent and reservoir thickness of 40-50 feet (Houseknecht and McGilvery, 1991; Perry, 1995). The Spiro was deposited within deltas in a stable shelf setting and later subject to normal faulting and facies selective diagenesis (Houseknecht and McGilvery, 1991). The Spiro reservoir is trapped by the overlying Atoka shale, which serves as the source for the overlying Red Oak reservoir (Perry, 1995).

The Red Oak sandstone is a sublithic arenite of highly variable thickness and porosity of 12-20 percent (Houseknecht and McGilvery, 1991; Perry, 1995). Turbidite deposition of the Red Oak in slope channels was followed by diagenesis during burial, which had an irregular effect on porosity, enhancing some areas and destroying others (Perry, 1995). The best reservoir quality is found along the base of the depositional horizon in east-west channel trends (Houseknecht and McGilvery, 1991). Differences in reservoir characteristics between the Spiro and the Red Oak are largely due to unique tectonic influences, despite their close proximity. Isolated by decollements in the Atokan shale between reservoirs, the Red Oak was subject to orogen-related

deformation not affecting the Spiro (Houseknecht and McGilvery, 1991). Compression forced the Red Oak into a thrusted anticline, accounting for the structural element of the reservoir trap (Houseknecht and McGilvery, 1991).

Figures

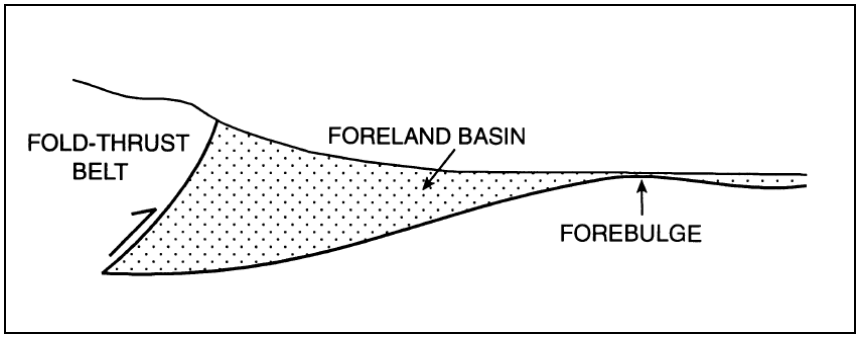

Figure 2.1: Simplified cross-sectional schematic of foreland basin formation associated with orogenesis (image modified after DeCelles and Giles, 1996, and used in accordance with Fair Use policy).

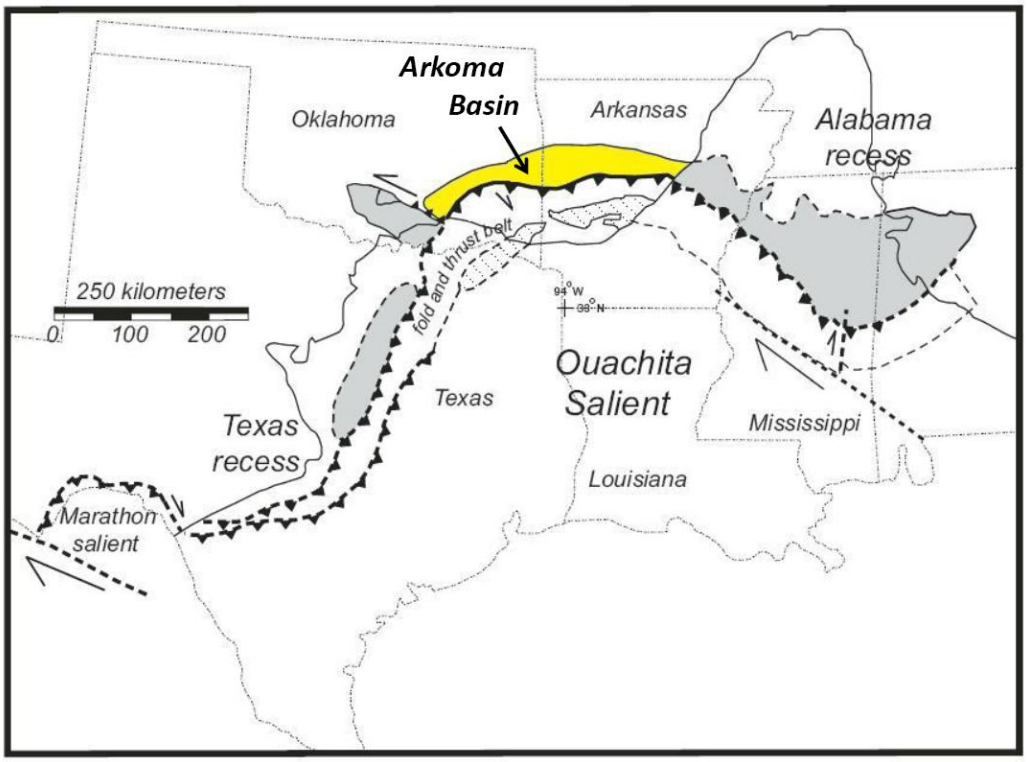

Figure 2.2: Location of the Arkoma Basin (highlighted) relative to the Ouachita-Marathon orogeny on the SE margin of North America (image modified after Whitaker and Engelder, 2006, and used in accordance with Fair Use policy).

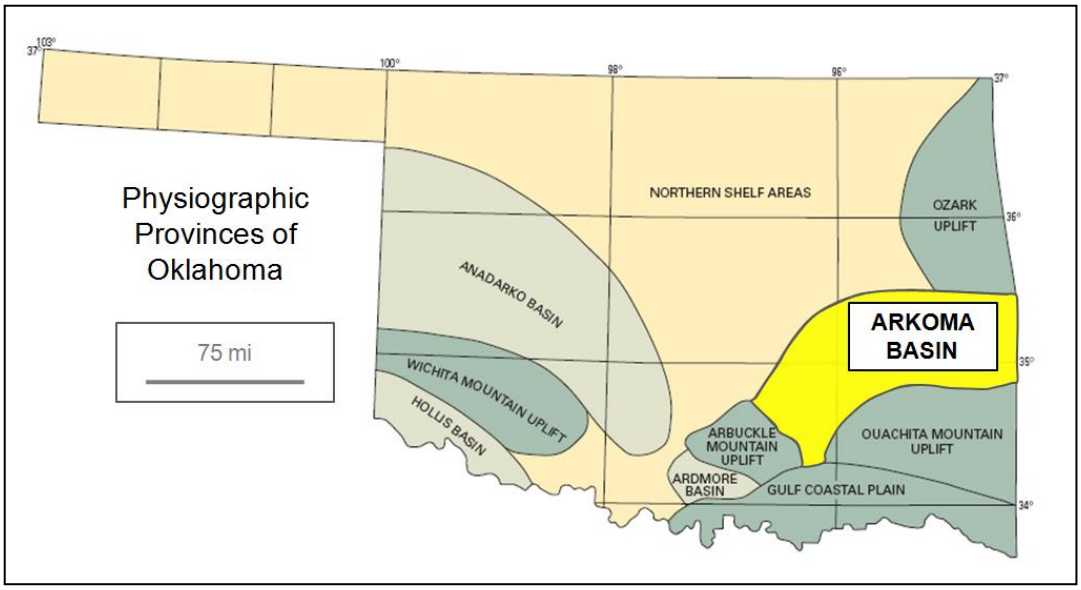

Figure 2.3: Location of Arkoma Basin province in Oklahoma (image modified after Heran, Green, and Stoeser, 2003, and used in accordance with Fair Use policy).

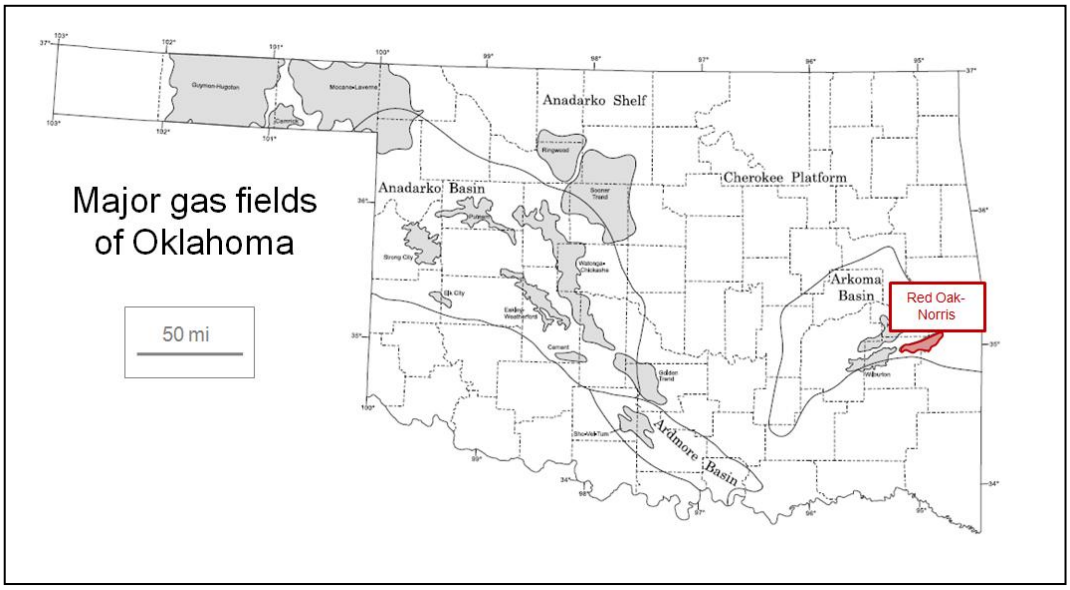

Figure 2.4: Location of the Red Oak-Norris gas field in the Arkoma Basin (modified after Boyd, 2005, and used in accordance with Fair Use policy).

Data

Real Data: Field Site and Collection

In November of 2007, Pinnacle Technologies, Inc. monitored an induced fracture treatment of the Red Oak sandstone reservoir, a hydrocarbon-bearing unit within the Arkoma Basin, at a field site in LeFlore County, Oklahoma. The survey area covers ~0.5 square-miles, with the horizontally-deviated injection well (Lowery #4-26H) running north-south and observation wells (Lowery #3 and Lowery #2-26), each containing an array of 12 three-component receivers, on either side of the injection well (Figure 3-1). While the injection well was drilled at mid-reservoir depth (inclining slightly with the dipping reservoir but averaging ~9300 feet), both receiver arrays are located above the reservoir. Receivers in Lowery #3 span a depth range of 8683.3 feet to 9088.6 feet at a regular spacing of 36.9 feet, and receivers in Lowery #2-26 span a range of 8275.9 feet to 8817.6 feet at 49.25-foot spacing.

The fracture treatment was completed in five successful stages (two additional stages were not completed) focused at near-regular spacing, averaging 454 feet, along the injection well. Treatment began at the north "toe" of the well and continued south for subsequent stages (Figure 3.2). Microseismic data for the survey were recorded for the 22-hour duration of the treatment and produced 15,918 seismic records sampled at 0.25 milliseconds for 0.5 seconds. Events range in magnitude from -2 to -4.

Real Data: Selection for Study

Less than ten percent of the seismograms recorded at the LeFlore County survey were ultimately used to obtain first-arrival traveltime picks for the hypocenter inversion. Because of the study's focus on the two-well case, only those events with potential to be recorded and

located by both observation wells were of interest. Therefore, records from stages 1 and 2 were not considered, as most events would be located near their associated stage locations, both outside the detection radius for the Lowery #3 well. Discarding stages 1 and 2 eliminated nearly half of the records collected from the experiment. The location of the remaining stages, 3, 4, and 5, in the general crosswell region, increased the likelihood of detecting their events at both wells. Examination of the 8549 records from these stages produced a working data set of 1197 higher-quality records (828 from stage 3, 241 from stage 4, and 128 from stage 5), in which first arrival time picks for events could be made for S-waves on both arrays and P-wave picks could be made on at least one array. The small magnitudes of events combined with large distances (~1600 feet) to receivers resulted in low signal relative to noise for P-wave arrivals, making them difficult to detect for most events. Since P-wave arrival times were available at both wells for only 30% of the 1197 events, S-wave data (picks and starting velocity model) were used for the hypocenter inversion rather than P-wave data or joint P- and S-wave data.

Gamma ray and sonic logs (Figure 3.3) were obtained from test wells near the survey. For the sandstone reservoir, they indicate a P-wave velocity (V_p) of ~15,000 ft/s and S-wave velocity (V_s) of ~8600 ft/s. Overall background velocities for the logs, including predominantly shale units both overlying and underlying the reservoir, remain reasonably uniform with an average V_p value of ~12,000 ft/s and V_s of ~7000 ft/s.

Real Data: Preparation for Inversion

Arrival times for the 1197 relatively high-quality records were picked manually using SeisPT, a proprietary microseismic processing program developed by Pinnacle (Figure 3.4). Each record contains 24 three-component seismic traces, with traces 1-12 corresponding to

receivers in the Lowery #3 well and 13-24 corresponding to those in the Lowery #2-26 well. Records are multi-component to show the full, three-dimensional receiver response. Amplitude gain and bandpass filtering (typically 31-500 Hz) were applied to all records to enhance signal-to-noise for improved picking. Picks were made at the onset of the signal on all possible traces for each arrival. The average picking error is estimated to be ~3.1 ms.

SeisPT calculates event locations based on the time picks and a user-defined velocity model. For this study, a simple, one-dimensional model, comprised of constant-velocity blocks based on the sonic log (Figure 3.5), was provided by Pinnacle. Because hypocenter inversion is more stable with smoothed models (Hole et al., 2000), a new, one-dimensional model was created by applying a series of moving average filters of different lengths (20, 50, and 100 feet) to the sonic log (Figure 3.5). This smoothing removed the sharp contrasts and oscillations of multiple frequencies that existed in the raw log, while retaining the significant velocity structure. A model volume of 1700 feet x 2600 feet x 1800 feet was defined. Event locations and time picks were exported from the software and converted from cylindrical coordinates to Cartesian coordinates for use as starting locations in the two-well hypocenter inversion (Figure 3.6).

Synthetic Data: Creation for Supplemental Investigations

Synthetic data were calculated to allow control in hypocenter location tests and enhance understanding of behaviors observed in the real data inversions. The synthetic survey geometry (model dimensions and receiver locations) is the same as that for the real data, but the true hypocenters and velocity model were simplified. This ensured error-free input data for comparison with results using real data.

Locations for true hypocenters were defined at 50-ft spacing throughout the entire model volume, except on faces (Figure 3.7). This dense arrangement of earthquakes, totaling 58,905, was designed to expose any geometry dependencies in results. A constant-velocity model was used to simplify the calculation of time picks and interpretation of results. A velocity of 7000 ft/s was chosen to approximate the average V_s encountered along raypaths through the real data model. With known event locations, receiver locations and seismic velocity, error-free travel times were easily calculated along straight raypaths for all hypocenters.

Figures

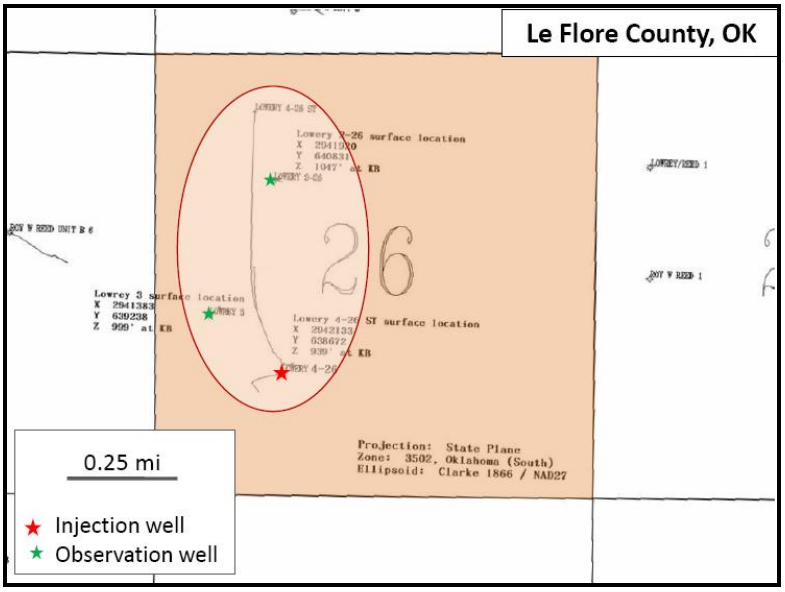

Figure 3.1: Map view of survey location in LeFlore County, OK (image used and modified with permission of Pinnacle Technologies, Inc.).

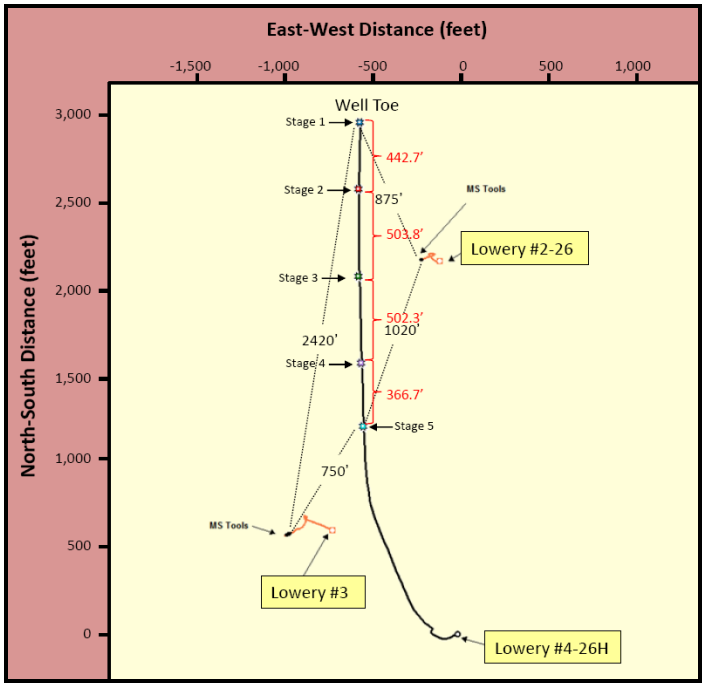

Figure 3.2: Map view of survey in detail (image used and modified with permission of Pinnacle Technologies, Inc.)

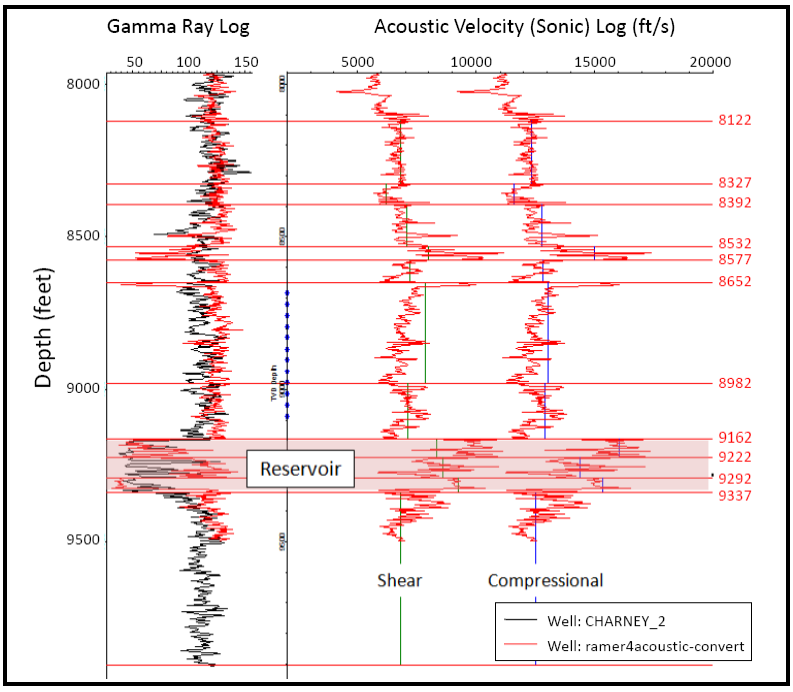

Figure 3.3: Gamma ray and sonic logs obtained for LeFlore County survey (image used and modified with permission of Pinnacle Technologies, Inc.). S-wave velocity is computed from the sonic (P-wave) data.

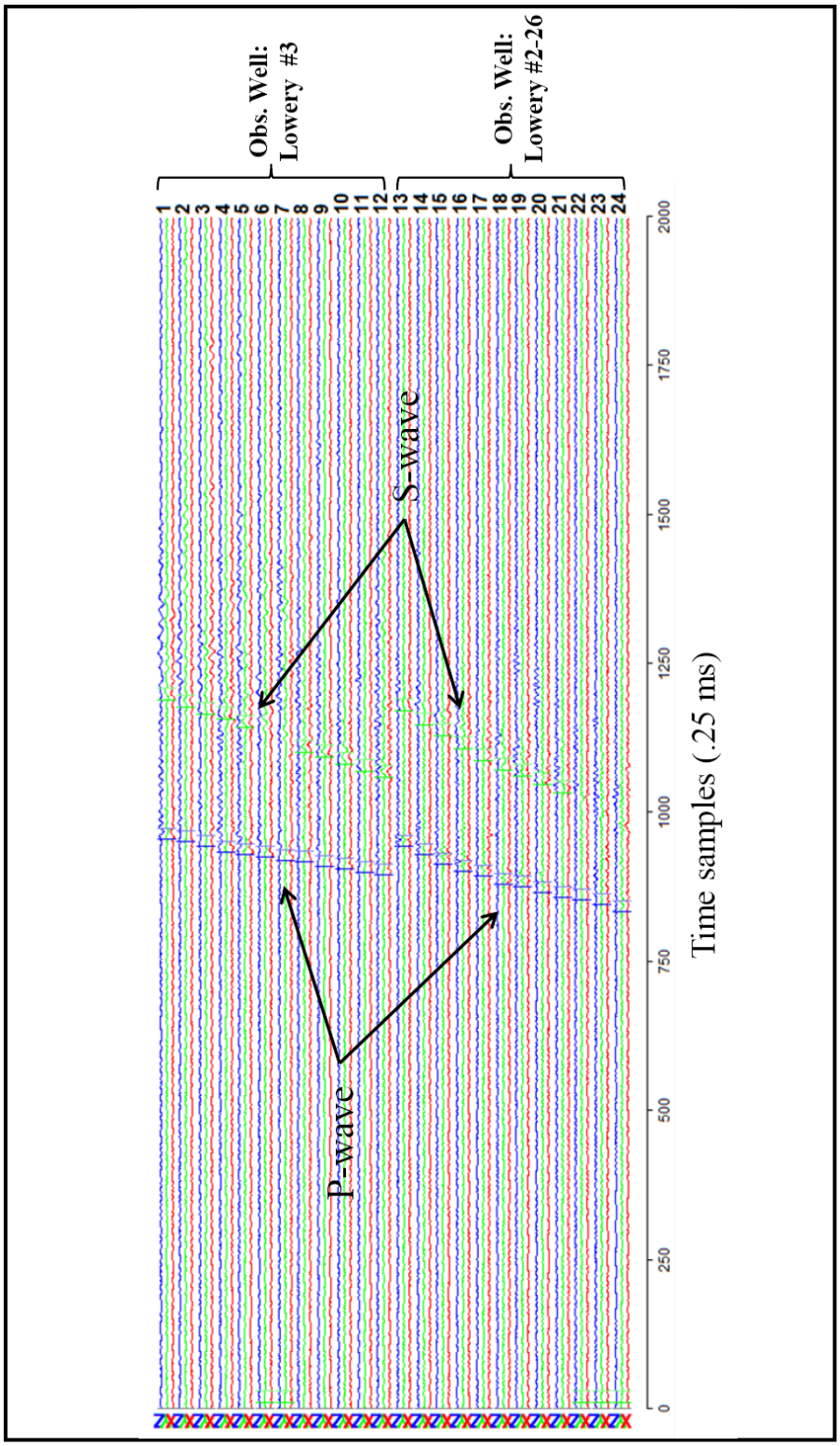

Figure 3.4: High-quality seismic record showing arrival time picks for P-waves (blue) and S-waves (green) on 24 three-component traces in two wells. Red, blue, and green traces display East-West, North-South, and vertical components of motion, respectively.

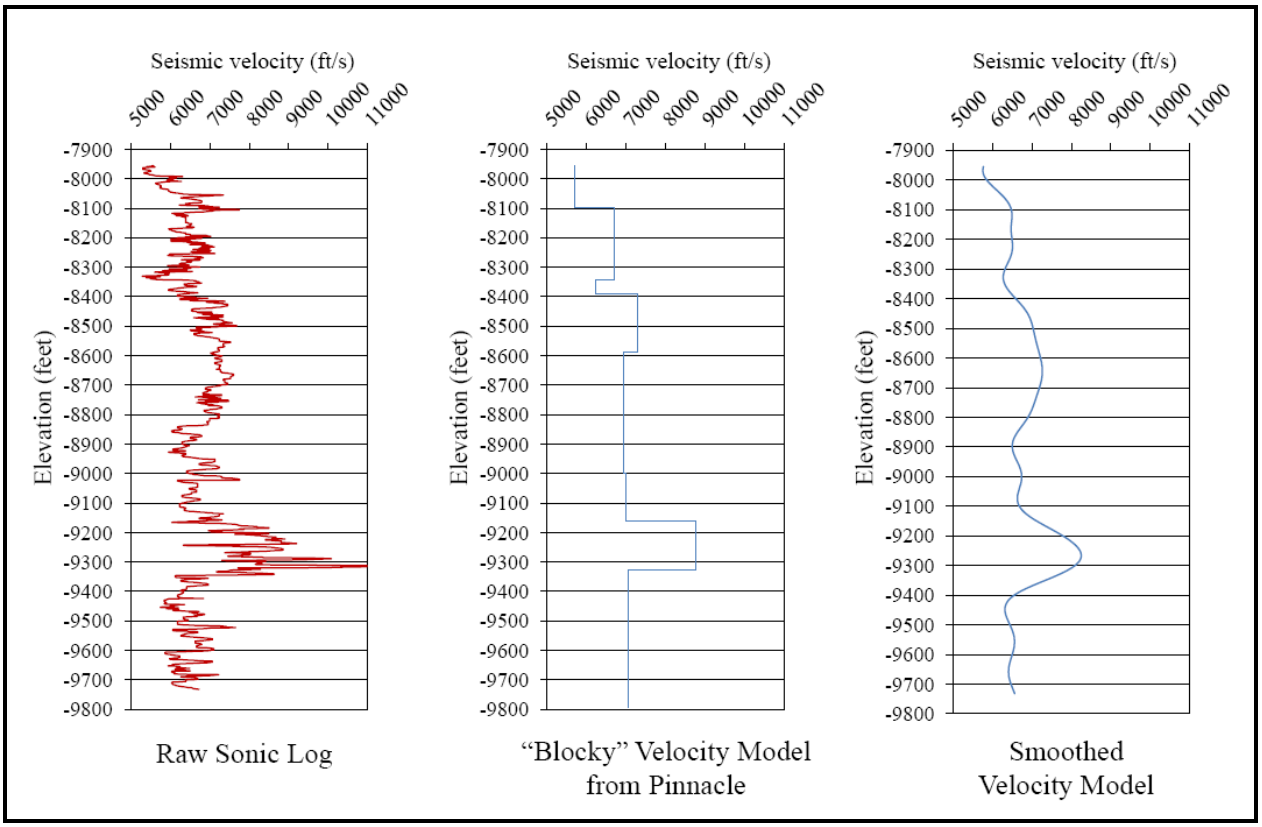

Figure 3.5: Comparison of Pinnacle's constant-velocity block model (center) and smoothed model used in hypocenter inversion (right), both derived from the raw sonic log (left). The high-velocity reservoir (9170-9340 feet) is a prominent feature in the log and the models. The smoothed model was obtained by applying a 20-ft moving average filter to the raw log 5 times, followed by a 50-ft filter 5 times, and a 100-ft filter once; this series of filters was necessary to smooth the several frequencies of oscillations and sharp contrasts present in the raw sonic log.

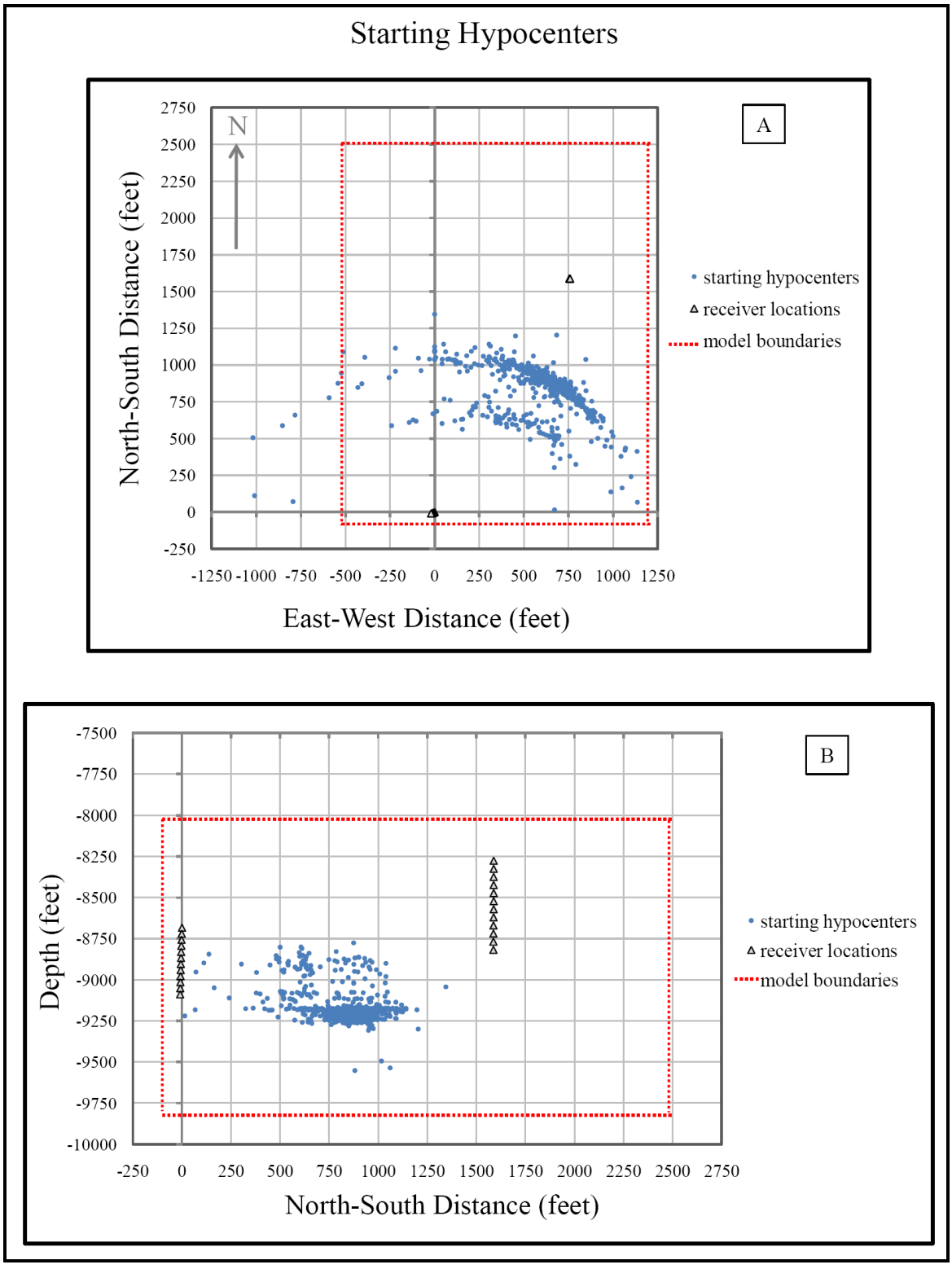

Figure 3.6: Starting hypocenters as exported from SeisPT in map view (A) and North-South cross section (B). The red box is the model volume for the two-well hypocenter inversion.

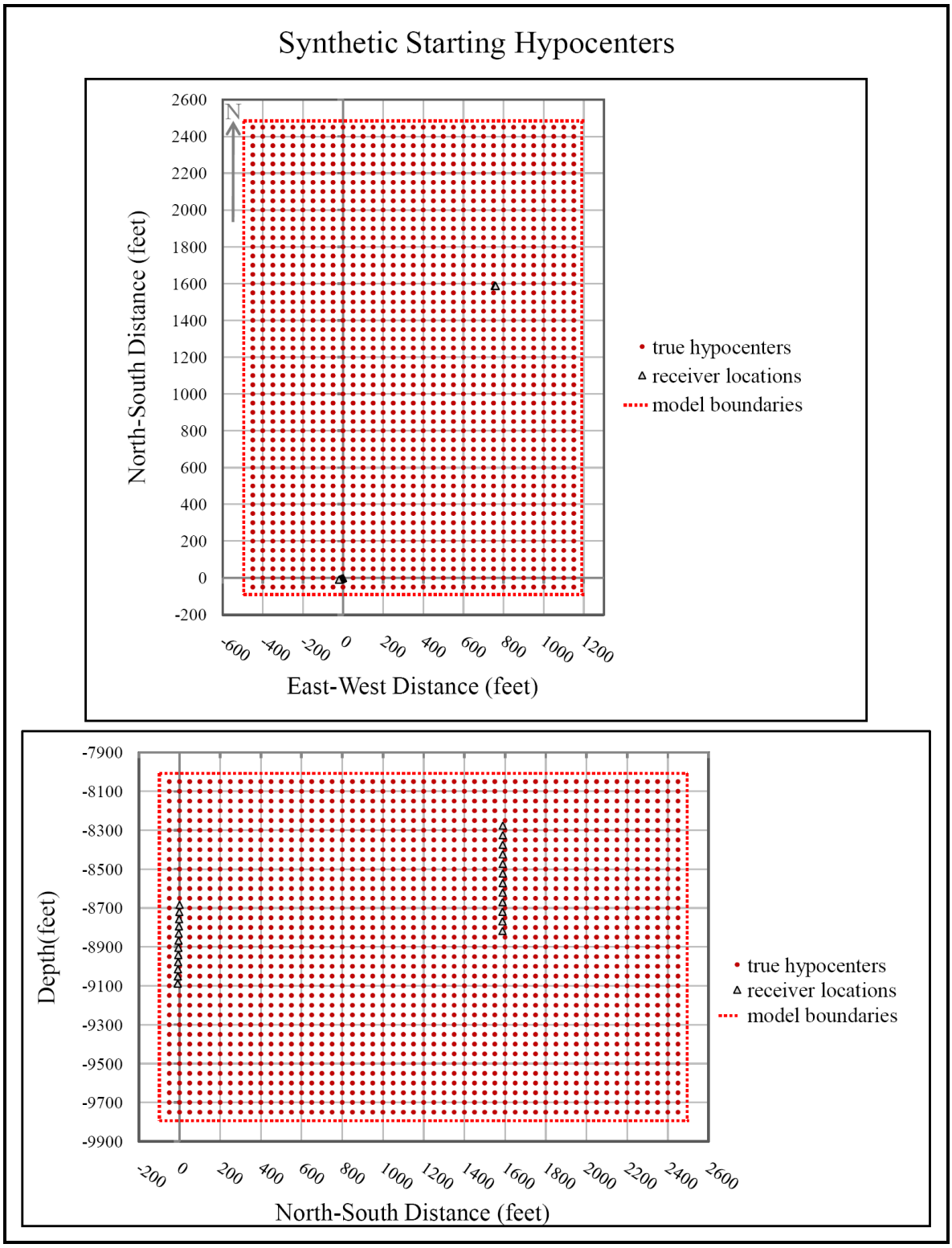

Figure 3.7: Synthetic starting hypocenters, "gridded" at 50-ft spacing, in map view (A) and North-South cross section (B).

Analysis

Original Motivation

The initial research objective was to apply a full earthquake tomography algorithm to improve absolute event locations and seismic velocity structure for the two-well case. Incorporating information from a second well can constrain the large azimuthal errors on earthquake locations obtained with a one-well solution and can also provide seismic velocity details from the crosswell region to improve the velocity model beyond one dimension. Accurate earthquake locations and velocity structure improve overall characterization of a reservoir and can also provide insight into the fracture treatment process.

Method

The hypocenter location algorithm of Hole et al. (2000) was used to invert the data in all investigations. Travel times are calculated in a three-dimensional velocity model employing a finite-difference solution to the eikonal equation (Hole and Zelt, 1995) that improves upon the algorithm of Vidale (1990). For each source, travel times are calculated to all grid nodes within the fixed velocity model. The code is able to simultaneously calculate times to a large number of receiver locations for a single earthquake, which offers a computational advantage over other relocation algorithms based on traditional raytracing. Given that travel times and rays are reciprocal between sources and receivers in a fixed model, it becomes practical to treat the relatively small number of receiver locations as sources and the large number of earthquakes as receivers. Because sources and receivers are not required to be located at model grid nodes, precise travel time calculations that account for time spent within the cell containing a given earthquake are necessary. This precision is achieved using tri-linear interpolation, which is the

interpolation in all three spatial dimensions averaged over the eight grid nodes surrounding the cell containing a given earthquake (Beale, 2004).

The hypocenter location algorithm, assuming a known velocity model, determines the misfit between calculated phase arrival times and observed arrival times to invert for updated hypocenter spatial coordinates, X, Y, and Z, and origin time, T (Hole et al., 2000). The linearized approximation of the relationship between time and hypocenter location (the Frechet derivative) uses the ray direction and velocity at the location of the initial hypocenter. Misfits calculated at all stations for all earthquakes are assembled and reorganized as matrices of linear equations for each earthquake. Singular value decomposition is used to invert the matrices and obtain least-squares corrections for the spatial coordinates and origin time of each earthquake hypocenter. As a quality control measure, the code rejects any earthquakes located at fewer than four stations or any earthquakes whose matrices contain eigenvalues smaller than a specified threshold. Times and matrices are recomputed for the new hypocenters and inverted iteratively solving the nonlinear inversion problem. With good data, the hypocenters converge to a final solution in 3-4 iterations.

The tomography algorithm of Hole et al. (2000) updates an earlier velocity tomography algorithm (Hole, 1992) to solve alternately for hypocenter locations and velocity structure in an iterative scheme that approximates simultaneous inversion of the traveltime data. Because the linearized inversions for the two unknowns remain independent, the user may fix either the locations of the hypocenters or the velocity model or may design a weighted convergence scheme to solve for both hypocenter locations and velocity structure. This flexibility allows the user to explore the trade-off that exists between these unknowns and the associated range of non-unique solutions for a given data set. The ability to explore the nonlinear hypocenter-velocity

model trade-off is an advantage of Hole's algorithm over truly simultaneous inversion and was an additional intended goal for the original study.

Two-well Real Data Hypocenter Inversion

The starting hypocenter locations exported from SeisPT display radial and other geometric artifacts (Figure 3.6). Because of this undesirable effect, an initial hypocenter inversion was conducted to improve event locations intended for use in the joint velocity and hypocenter tomography algorithm. Only S-wave picks were used in the inversion, along with the smooth velocity model of Figure 3.5 extrapolated to three dimensions over a 1700 ft x 2600 ft x 1800 ft model volume with a grid cell size of 10 feet.

This inversion resulted in a significant number of event locations diverging out of the model volume (Figure 4.1). A few events moved deeper, below the model volume, but many moved large horizontal distances, up to tens of thousands of feet. A single linearized iteration of the nonlinear hypocenter relocation algorithm moved 421 events, 35% of the original 1197, out of the model volume, removing them from further iterations. After a second iteration, 887 events had left the model, leaving only 310, or 26%, of the original set.

Movement for most events appeared to be systematic in a preferred direction nearly perpendicular to the crosswell direction. For comparison, the line truly perpendicular to that between wells is displayed in Figure 4.1. However, the seemingly biased orientation of relocated events may be a true geologic phenomenon, governed by fracture network geometry and the local stress field. In support of this idea, the trend of relocated events is roughly perpendicular to the horizontal treatment well, which is often intentionally drilled at a high angle to natural

fractures for a known stress field. This orientation maximizes permeability pathways into the well.

A test of the relocation algorithm was conducted using error-free synthetic travel times for synthetic events comparable to the real event locations. This test eliminated software bugs as a source of error in the unexpected relocation solution, pointing instead to an inherent lack of hypocenter constraint in the two-well problem using only S-wave times. The remainder of this study is a more detailed and thorough investigation of this problem.

Damping Factor

Many hypocenters relocate outside of the model volume in the first iteration of inversion, removing them from subsequent iterations which could return them to the model. In an effort to retain hypocenters within the model space and slow divergence, damping factors ranging from 10^{-6} to 10^{-2} times the largest eigenvalue were tested in the inversion. Damping limits the size of steps that hypocenters can take for iterations of the inversion, preventing hypocenters that take indirect paths to their final locations from accidentally leaving the model along the way. Because the hypocenters that were observed to accidentally move outside the model in the first iteration often moved very large distances, the largest damping factor, 10^{-2}, was required to sufficiently restrict step size. This measure helped retain hundreds of hypocenters in the model and in the final inversion solution (Figure 4.2). Notice that damping does not change the solution other than retaining hypocenters that left the model on accident. General location patterns and geometric eccentricities are the same for the damped and undamped solutions. Damping was applied to all inversions used in investigations of the real data.

Revised Motivation

The geometric anomalies observed in early attempts to improve hypocenter locations were unexpected and motivated the remainder of this study. The focus of research was redirected to explore this problem and specific sources of error on hypocenter locations. Further investigations of the real data were combined with synthetic data tests to determine how the accuracy of the velocity model, starting hypocenters, receiver geometry, and traveltime picks affect hypocenter location. A better understanding of the location error observed on the real data could be helpful in improving and optimizing the collection and analysis of other earthquake data sets.

Figures

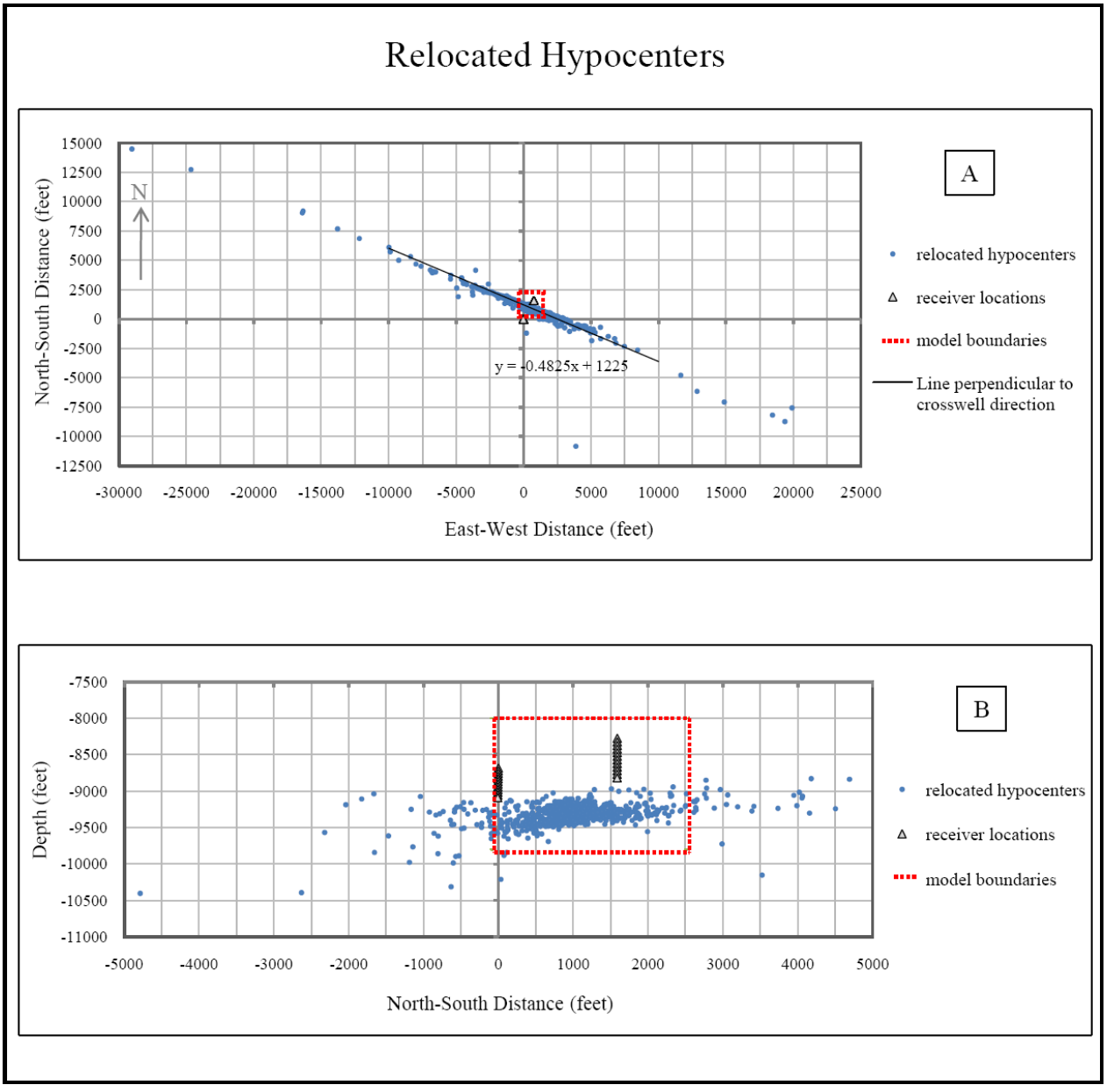

Figure 4.1: Anomalous hypocenters after a single relocation iteration in map view (A) and North-South cross section (B). The trend line in (A) corresponds to the direction perpendicular to the crosswell direction. Note the large scale of the map and relatively small size of the model volume (red box).

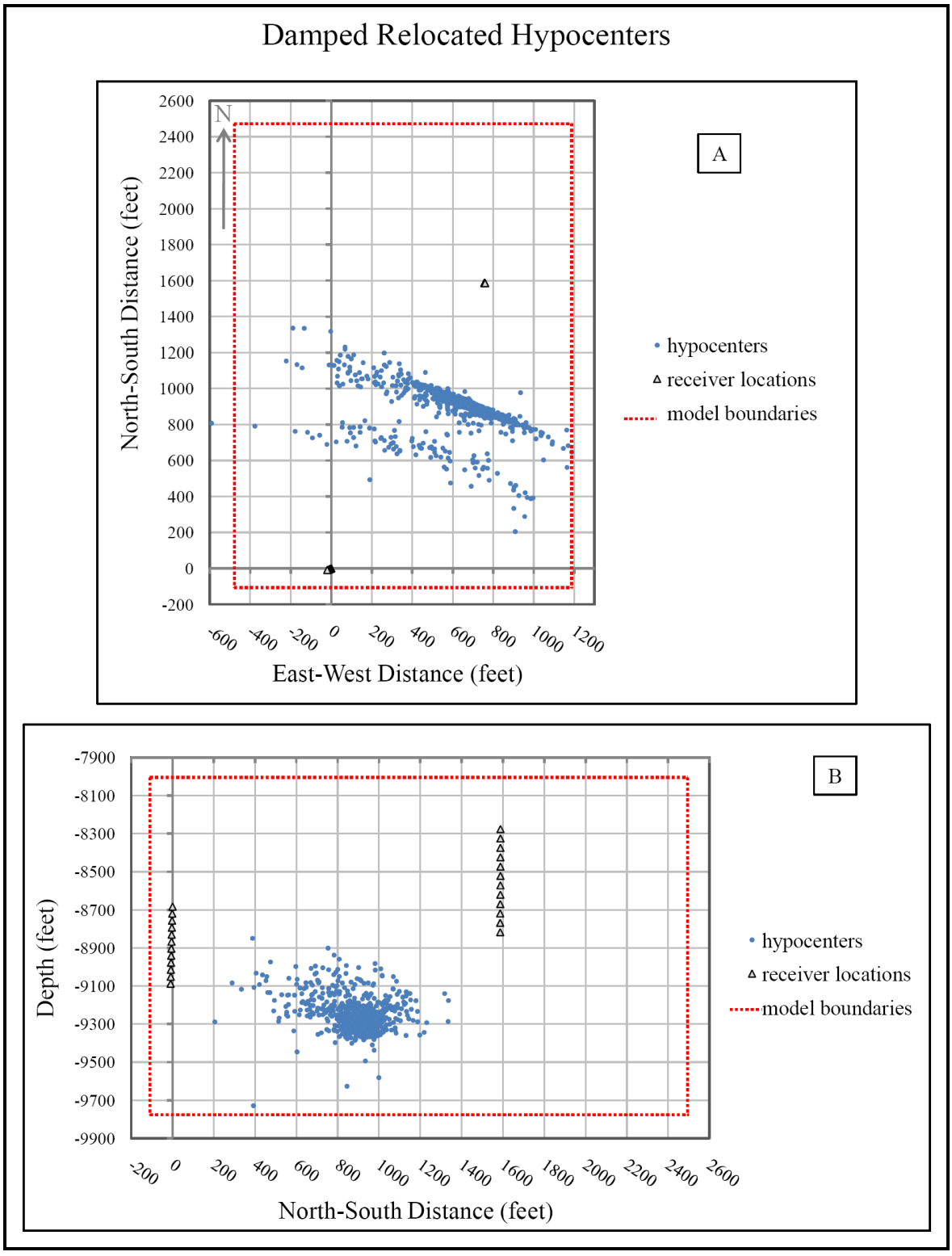

Figure 4.2: Hypocenters after a single damped relocation iteration in map view (A) and North-South cross section (B).

Investigation 1: Effect of Velocity Model

The earthquakes unexpectedly relocated to greater depths with each iteration of the inversion. Initial hypocenter locations were mostly within or above the reservoir (Figure 5.1, A and C), but, upon inversion, migrated well below the reservoir (Figure 5.1, B and D). Furthermore, plotting hypocenters for several successive iterations suggests a systematic, hyperbolic path that many hypocenters take when converging below the reservoir (Figure 5.2). Tracking the paths of individual earthquakes confirms this suggestion (Figure 5.3).

Because the induced fracture treatment was conducted within the Red Oak reservoir, hypocenters should relocate primarily within the reservoir. The fact that they systematically relocate much deeper could be due to a refraction effect of the high-velocity reservoir; this would cause the ray path determined by raytracing in the inversion code to differ from the path determined by time picks. The effect of a false velocity model upon hypocenter locations is known to be profound (Giardini, 1992; Hole et al., 2000).

Four new velocity models were created to test the effect of velocity structure on hypocenter location. All five models used were based on the sonic log data, smoothed to varying degrees (Figure 5.4). The original model (Figure 5.4, C) had been obtained by applying a 20-ft moving average filter to the raw log five times, followed by a 50-ft moving average filter five times, followed by a 100-ft moving average filter once. This smoothing scheme was designed to preserve the significant structure seen in the raw log but remove most of the sharp contrasts to stabilize the inversion. Two rougher models were built by applying a 40-ft moving average filter to the sonic log only once (Figure 5.4, B) and by recreating the constant-velocity block scheme of Pinnacle's model (Figure 5.4, A). Two smoother models were built by applying a 100-ft moving average filter to the sonic log, followed by a 200-ft moving average filter (Figure 5.4,

D), and by using the average of all of the sonic log velocities within the model range as the value for a constant-velocity model (Figure 5.4, E). All models were tested in the relocation inversion, keeping other input data and inversion parameters the same.

The numbers of earthquakes retained through iterations of the inversion varied significantly among the five models and are listed in Table 5.1 for all 60 iterations. Increased velocity structure improves earthquake retention in the relocation solution, and conversely, increased smoothing causes more earthquakes to diverge. The fact that Pinnacle's block model with sharp velocity contrasts (Model A) is most successful at retaining earthquakes is somewhat counter-intuitive, as smoothing is usually considered a tool to make inversion more stable. Additionally, the block model also helps hypocenters converge within the reservoir (Figure 5.5). Although many still diverge along a hyperbolic path, 33% of the earthquakes included in the inversion after 20 iterations are located in the reservoir. The higher earthquake retention and better convergence within the reservoir obtained with the block model (A) made its solution the most desirable in the velocity model test. However, most earthquakes still move systematically downward and outward in this result. This demonstrates that the geometric bias in hypocenter locations can be improved, but not resolved, with an improved velocity model and indicates other factors governing the anomalous relocation behavior.

Figures

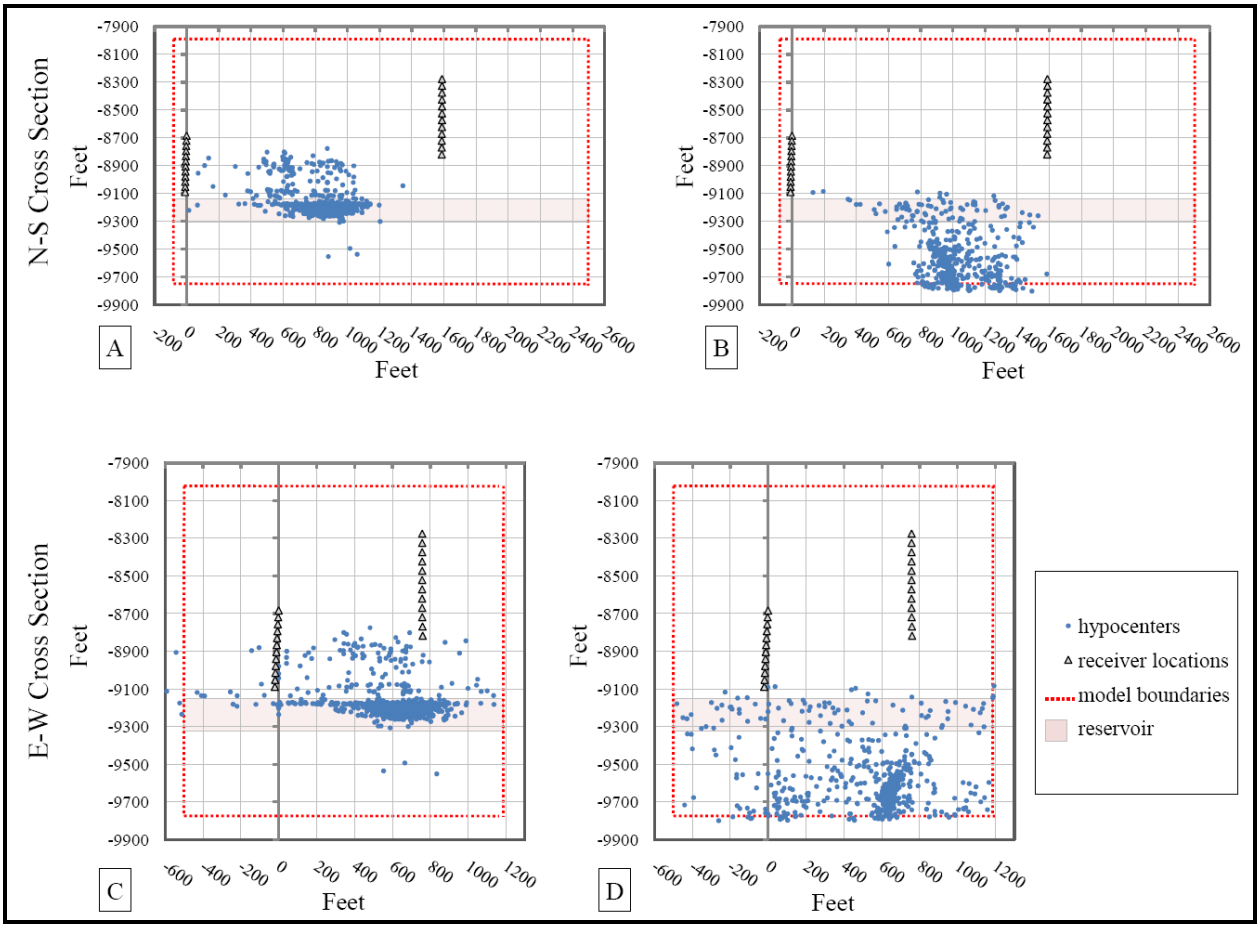

Figure 5.1: Migration of events in depth, shown by comparison of hypocenters in North-South cross section at starting locations (A) and final locations (B) and in East-West cross section at starting locations (C) and final locations (D).

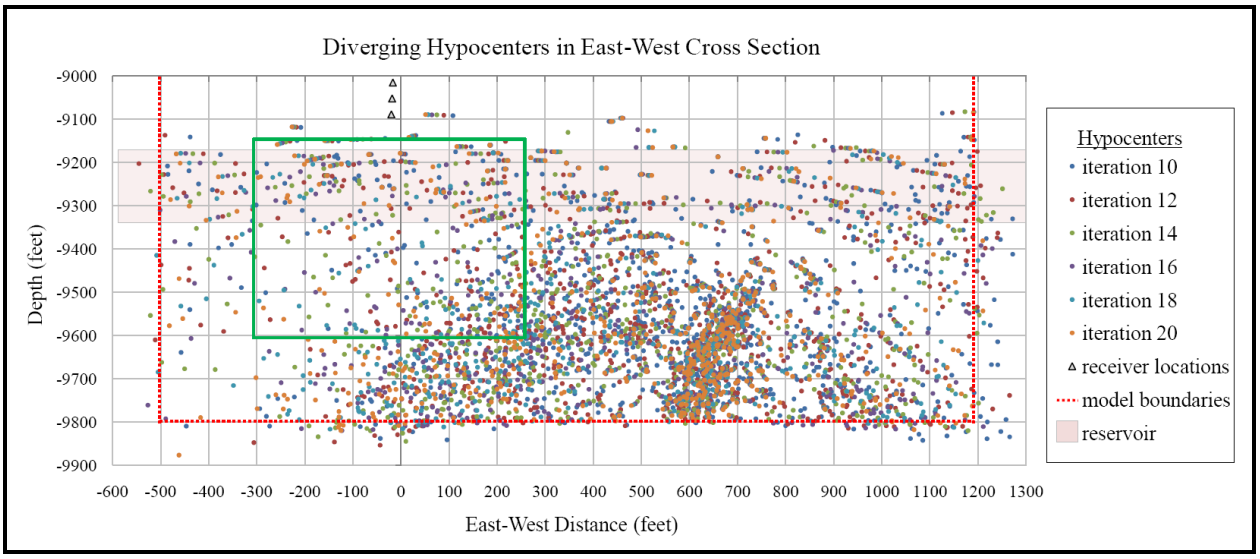

Figure 5.2: East-West cross section of hypocenters from several successive relocation iterations shows many events converging outward and downward along a hyperbolic path. The paths of earthquakes in the green box are displayed for the same six iterations in zoomed view in Figure 5.3.

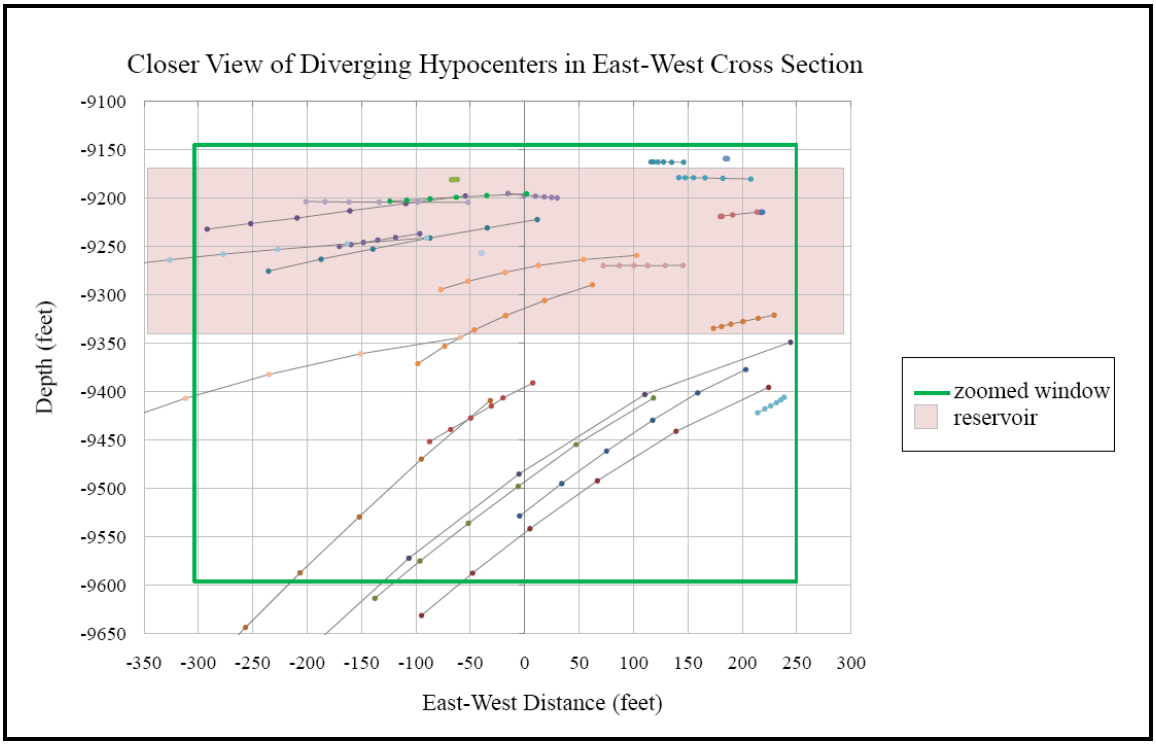

Figure 5.3: Zoomed-in view of earthquakes diverging along hyperbolic paths in East-West cross section. Hypocenter locations for a single earthquake are tracked through several iterations of the inversion and displayed as points of the same color, connected by a line indicating the travel path. The green box outlines the same area as in Figure 5.2.

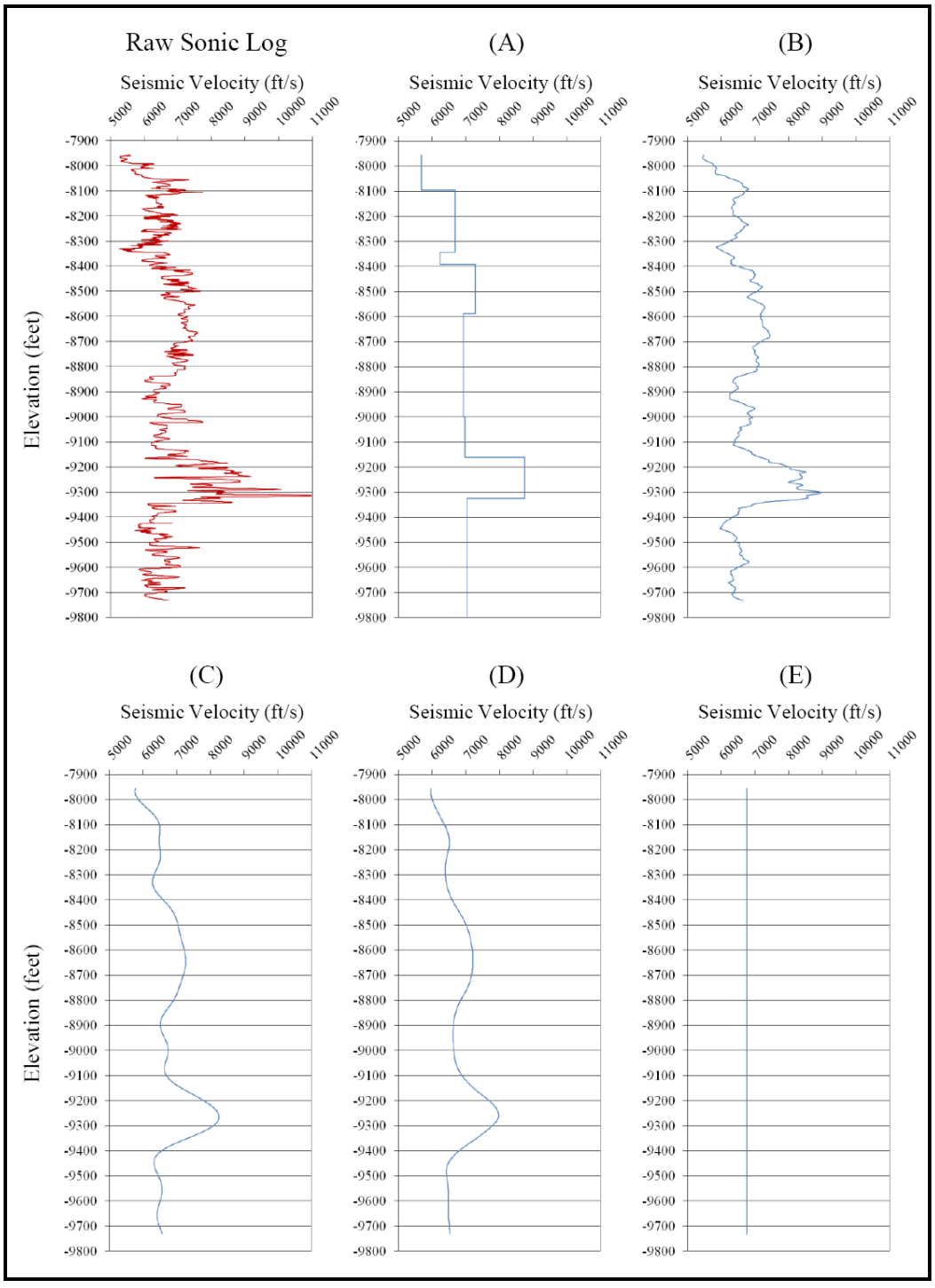

Figure 5.4: Raw sonic log (upper left) compared to five velocity models based on log. Model (A) is comprised of constant-velocity blocks and is a recreation of Pinnacle's model. Model (B) is the raw log with a 40-ft moving average filter applied to retain significant and detailed structure. Model (C) was used in the original test and is the raw log with a series of moving average filters applied to retain less structure. Model (D) is the raw log with 100-ft and 200-ft moving average filters applied to retain less structure. Model (E) is a constant velocity model where the velocity value is the average of the raw log.

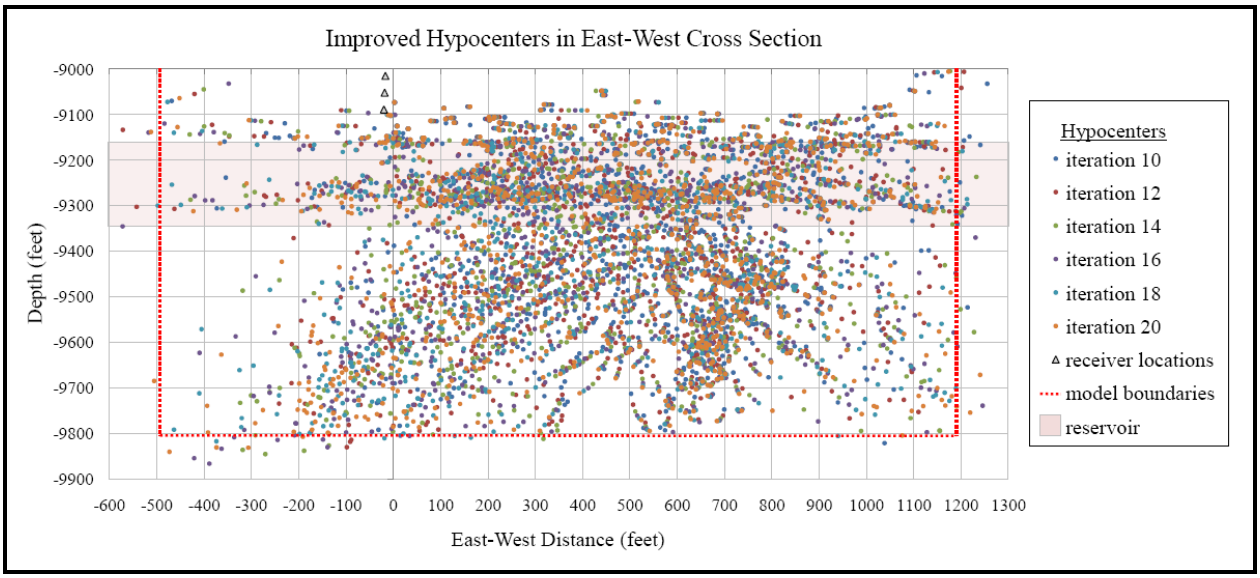

Figure 5.5: East-West cross section of improved hypocenters from several successive relocation iterations using Model A, based on Pinnacle's model of constant-velocity blocks. More earthquakes remain in the model space, and more converge within the reservoir. However, even in this preferred case, most earthquakes travel downward and outward, demonstrating that the geometric bias in hypocenters can be improved, but not resolved, by an improved velocity model.

	roughest ← Model → smoothest				
Iteration	**A**	**B**	**C**	**D**	**E**
1	1186	1186	1186	1186	1186
2	1178	1182	1183	1180	1168
3	1168	1174	1172	1167	1121
4	1166	1168	1165	1156	874
5	1161	1163	1152	1133	460
6	1156	1153	1136	1057	271
7	1152	1136	1110	971	177
8	1147	1116	1068	860	137
9	1145	1103	1013	767	112
10	**1139**	**1083**	**958**	**700**	**90**
11	1131	1058	915	649	77
12	1122	1030	874	605	70
13	1113	1003	842	576	66
14	1103	975	811	542	62
15	1093	952	780	518	57
16	1081	937	755	501	51
17	1067	915	727	477	51
18	1051	896	705	461	49
19	1041	874	692	446	46
20	**1026**	**862**	**675**	**430**	**44**
21	1017	850	661	420	43
22	1007	840	652	410	41
23	994	836	639	403	41
24	980	829	628	396	41
25	966	821	619	391	40
26	958	811	615	387	39
27	949	806	605	381	39
28	940	798	597	378	39
29	935	788	590	373	38
30	**925**	**783**	**586**	**366**	**38**
31	921	778	579	363	38
32	919	772	574	361	37
33	910	770	571	357	36
34	905	768	563	352	36
35	896	766	558	350	35
36	893	764	552	347	35
37	890	758	549	344	35
38	888	757	544	343	35
39	886	752	541	341	35
40	**881**	**750**	**539**	**338**	**34**
41	876	750	535	336	34
42	875	748	531	334	34
43	870	746	531	334	34
44	869	744	528	332	34
45	867	743	525	330	34
46	866	741	522	330	33
47	864	739	520	327	33
48	861	738	517	326	33
49	860	736	517	326	33
50	**857**	**736**	**516**	**326**	**33**
51	855	735	514	325	33
52	848	733	514	325	33
53	846	732	514	325	33
54	844	731	513	324	33
55	840	730	512	323	33
56	838	730	510	323	33
57	837	730	509	323	33
58	836	729	508	323	33
59	836	729	508	321	33
60	**835**	**728**	**507**	**321**	**33**

Table 5.1: Numbers of earthquakes retained (out of the original 1197) through all 60 iterations of the hypocenter relocation inversion for each of the five models, A-E, tested (smoothing increases from left to right).

Investigation 2: Effect of Starting Hypocenter Locations

In the original inversion attempt, earthquakes quickly aligned perpendicular to the line between observation wells, as shown previously in Figure 4.2. Further iterations caused the hypocenters to move on paths along that line in map view and hyperbolic in cross section, as seen earlier in Figure 5.2. From this geometrical behavior, it appears that hypocenters converge to a best-fitting solution that is outside the model space. The systematic bias apparent in this behavior suggests that the relocation solution is not likely affected by starting hypocenter locations. To investigate whether this anomalous convergence behavior is indeed independent of starting locations, tests were conducted using both real and synthetic data sets.

Real Data Test

A test of the real data used a different set of starting hypocenters with all other input data the same. The fracture treatment was conducted in several stages, each focused at a different location along the injection well (Figure 3.2). All earthquakes used in the inversion were generated during the three treatment stages located in the between-well region (stages 3, 4, and 5). For this test, earthquakes were placed at the spatial coordinates of their associated stage locations, so that all starting hypocenters were at one of three locations. This set of starting hypocenter locations is compared with the original set obtained from SeisPT in Figure 6.1. Final hypocenter locations for both inversions are compared in Figure 6.2. The solutions are not identical, but strong similarities are apparent in both map view and cross section. Inversion using stage locations as starting hypocenters produced 612 converged hypocenters in the final solution, compared to 507 using starting hypocenters from SeisPT. Of the earthquakes retained

in each solution, 487 are common to both, meaning each contains earthquakes unique to that solution.

It is difficult to assess the degree of similarity between these solutions with confidence by visual inspection alone. Although it appears likely that common earthquakes are associated with common final locations, this is speculation, further complicated by the existence of unique earthquakes in each solution. To confirm the similarity of the solutions, a measure of the difference between solutions was determined by calculating the distance between a final hypocenter in one solution and its counterpart in the other, for all earthquakes common to both solutions. A summary of the results from this calculation is presented as a histogram in Figure 6.3. As the histogram shows, most final hypocenters are short distances (<10 feet) from their counterparts in the other solution. Outliers locate as far as 1833 feet from their counterparts but are few in number. This result supports the hypothesis that final hypocenter locations are independent of starting locations. To further test the hypothesis, a synthetic study was conducted to better isolate and examine the effect of starting hypocenters on the final location solution.

Synthetic Data Test

A synthetic study was designed to test the ability of the inversion to recover the true location of an earthquake for any possible starting location when all other input data are error-free. Eight hypocenter locations were defined as true locations for earthquakes (Figure 6.4). These eight were chosen to sample and explore a variety of location scenarios throughout the model space: closer to one well (locations 5, 6, 7, 8) versus nearly equidistant between them (locations 1, 2, 3, 4), near the line between wells (locations 1, 2, 5, 6) versus off line (locations 3, 4, 7, 8), at depth within the receiver range (locations 1, 3, 5, 7) versus true reservoir depth below

the receivers (locations 2, 4, 6, 8). For each true location, error-free traveltime picks were calculated to all receivers and used in the inversion. False starting locations were distributed at dense 50-ft spacing, vertically and horizontally, throughout the entire model volume. This array of 58,905 starting hypocenters was described previously and is shown in Figure 3.7.

Results of the synthetic study show that starting hypocenter location determined whether an earthquake converged in the final relocation solution or diverged out of the model. In order to converge, starting hypocenters must be within the volume of the model that is well-surrounded by receiver stations. This important finding is illustrated in Figure 6.5, where starting hypocenters that ultimately converged for a particular true location test are shown in pink and those that diverged are shown in gray.

When the true earthquake location was close to the line between observation wells, the hypocenters that did converge reached the true earthquake location (Figure 6.5). This was true regardless of the earthquake's location along the line between wells and regardless of its depth. Figure 6.6 tracks hypocenters converging to the true earthquake location over several iterations for one of these cases. This figure confirms the suggestion of early observations that hypocenters quickly converge to a line perpendicular to the between-well line and then take smaller steps along that line to a final location.

In cases where the true earthquake location was some distance from the line between wells, hypocenters converged to one of two minima (Figure 6.7). In these cases, one minimum was always the true earthquake location, while the other was located on the opposite side of the between-well line. Recall from Figure 1.3 (B) that traveltime data from two wells can result in two possible solutions for a single earthquake location. Here, minima create a line perpendicular to the between-well line but are not exactly symmetric to the receiver geometry, as they are not

equidistant from the between-well line. This could be due to asymmetry of the receiver arrays, which are mostly symmetric in map view but cover different depth ranges. Convergence to one minimum or the other is governed entirely by the location of a starting hypocenter relative to the between-well line (Figure 6.7). In general, earthquakes converge to the nearest of the two minima. Tracking a dual minima solution through several iterations, as shown in Figure 6.8, further illuminates the role of the between-well line in guiding hypocenters toward two distinct minima.

Figures

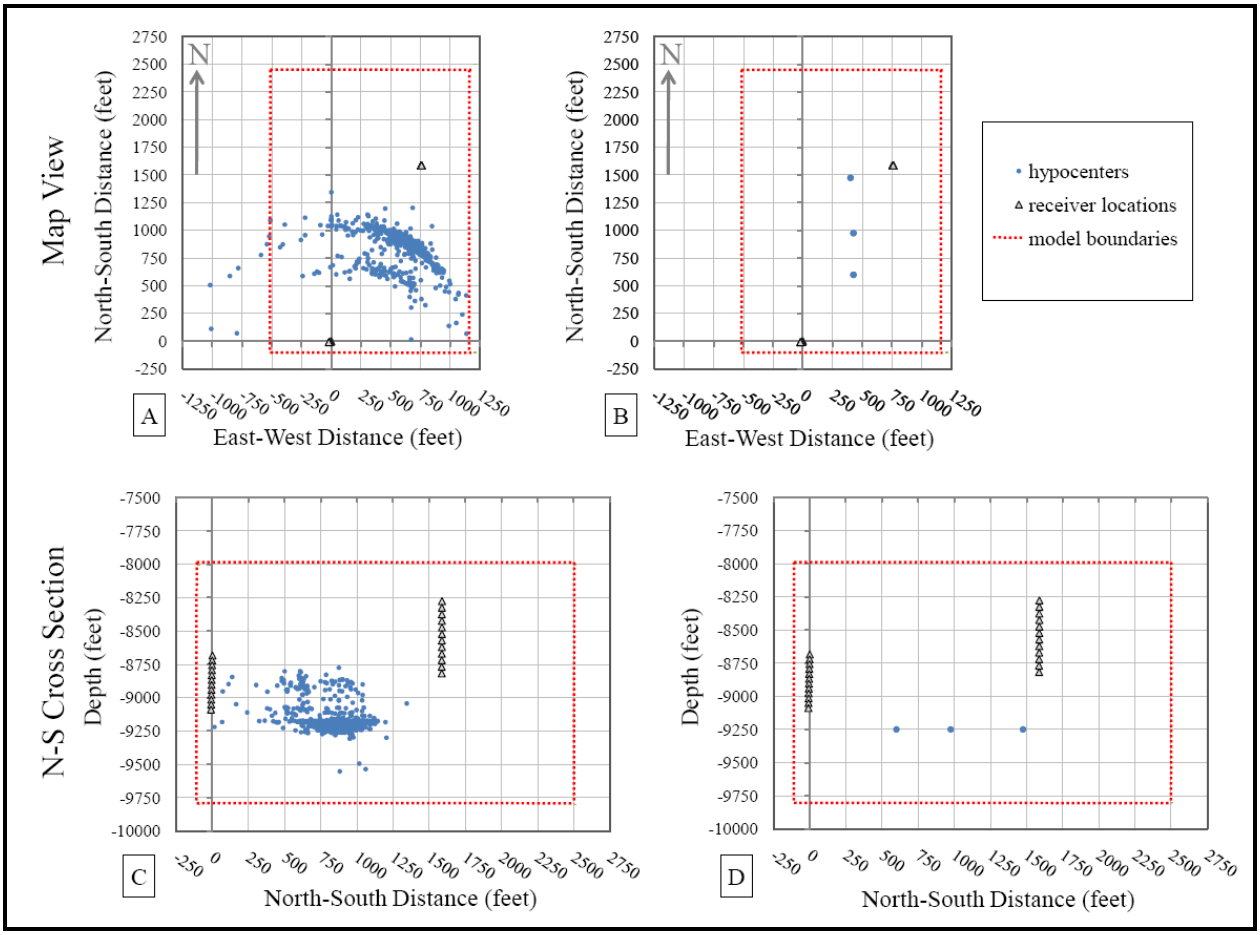

Figure 6.1: Comparison of starting hypocenters for real data test. Original hypocenters from SeisPT are shown in map view (A) and North-South cross section (C), along with new starting hypocenters at stage locations in map view (B) and North-South cross section (D). The stage locations are the same as those shown in the survey map in Figure 3.2 for treatment stages 3, 4, and 5.

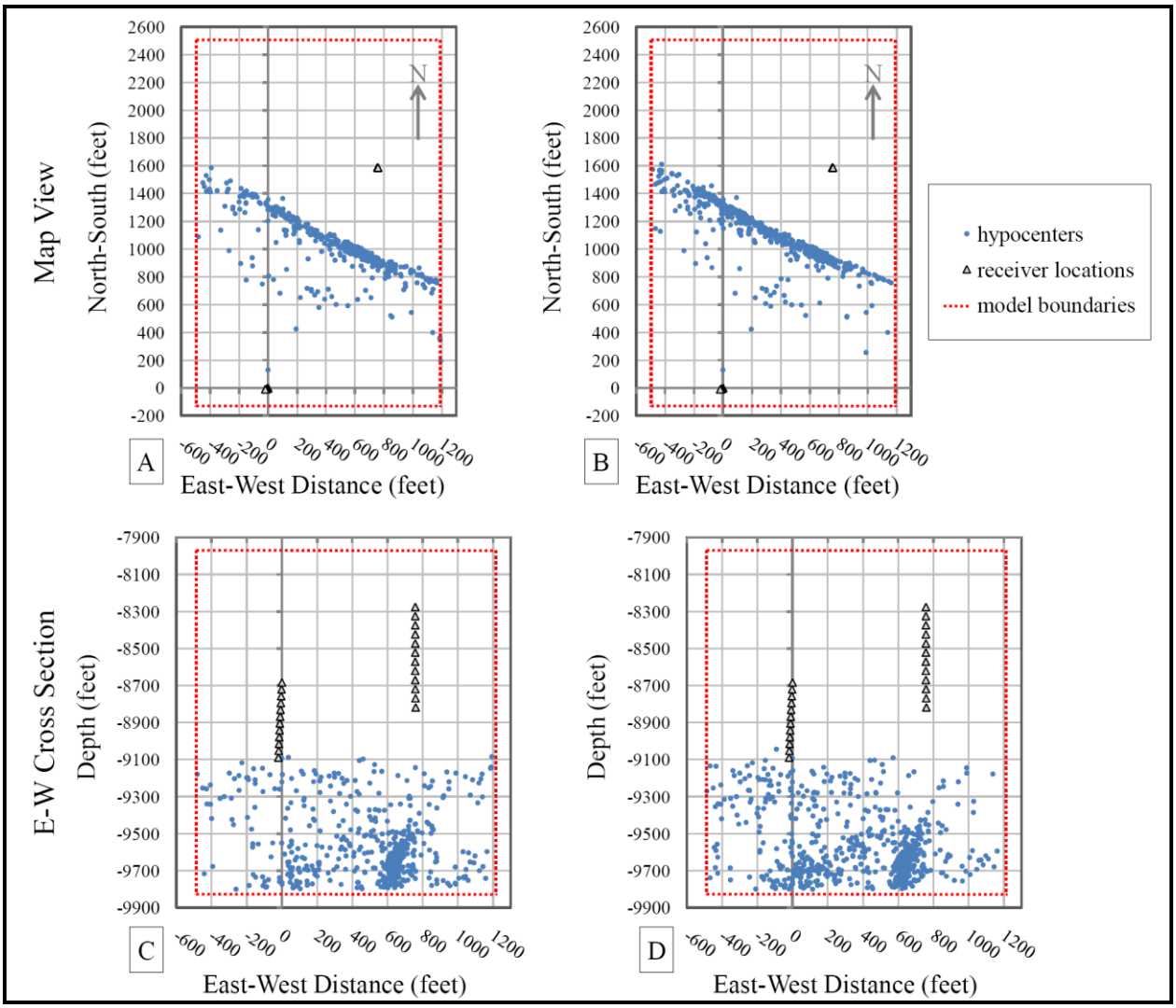

Figure 6.2: Final locations for the SeisPT hypocenters in map view (A) and East-West cross section (C) and for the stage hypocenters in map view (B) and East-West cross section (D). Solutions are not identical but show strong similarities in both views.

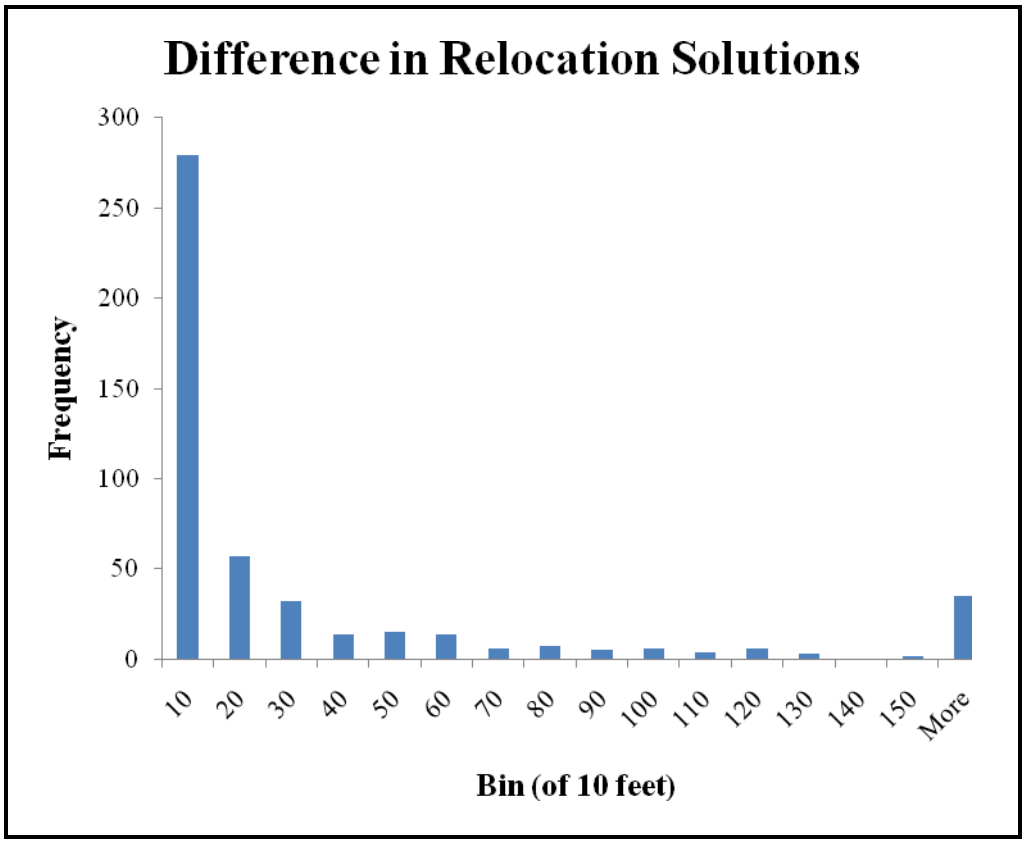

Figure 6.3: Histogram of difference between two relocation solutions, calculated as the distance between hypocenters from one solution and their counterparts in the other solution. A majority of hypocenter pairs (279 out of 485) are within 10 feet of each other. The "More" bin appears high due to outliers spread as far as 1833 feet from their counterparts, with all bins greater than 150 feet containing very small numbers of hypocenter pairs.

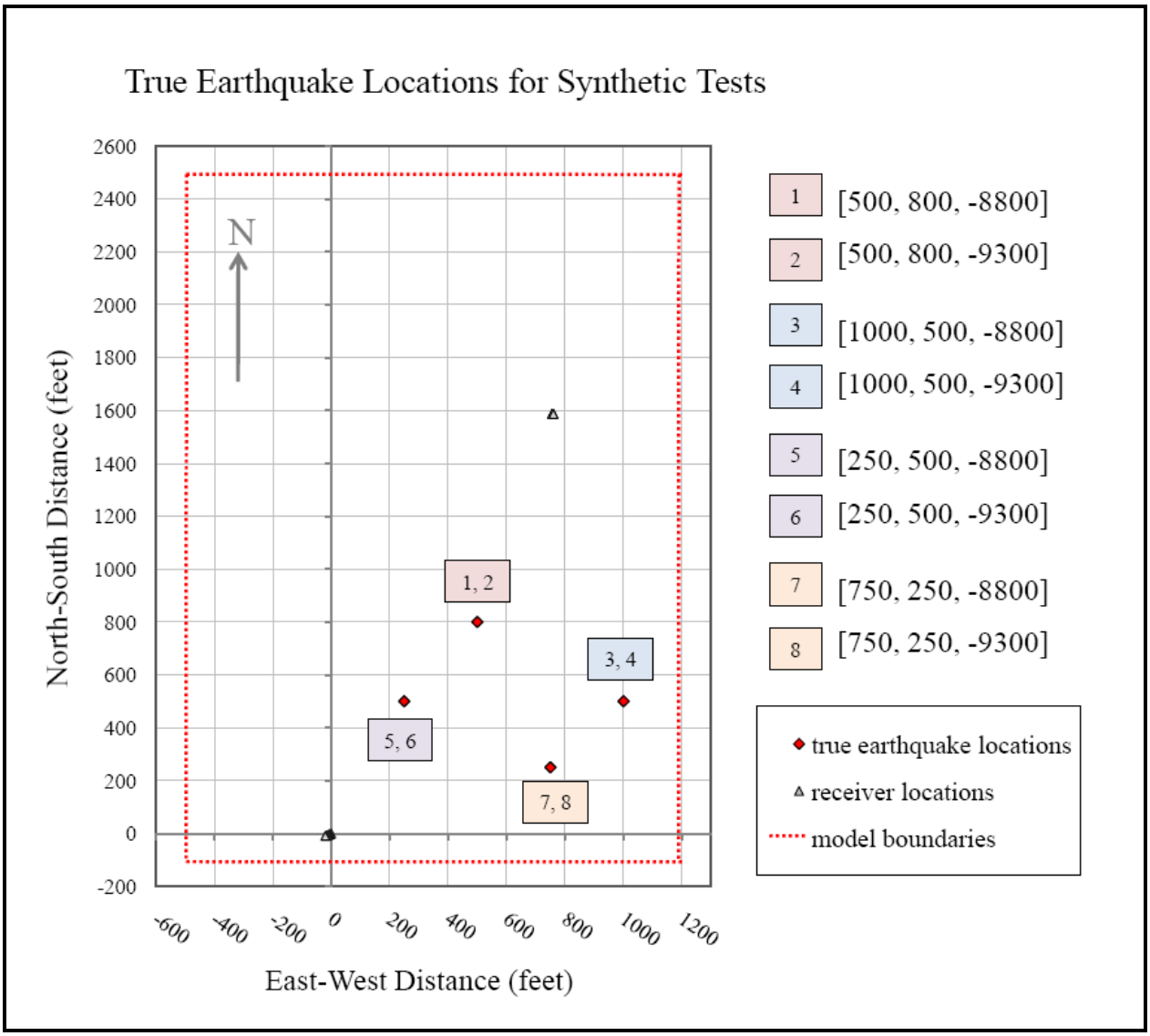

Figure 6.4: Map view of true earthquake locations for synthetic tests. Two earthquakes were defined at different depths for each of the four locations pictured. Spatial coordinates [X, Y, Z] for all eight earthquakes are displayed to the right of the map.

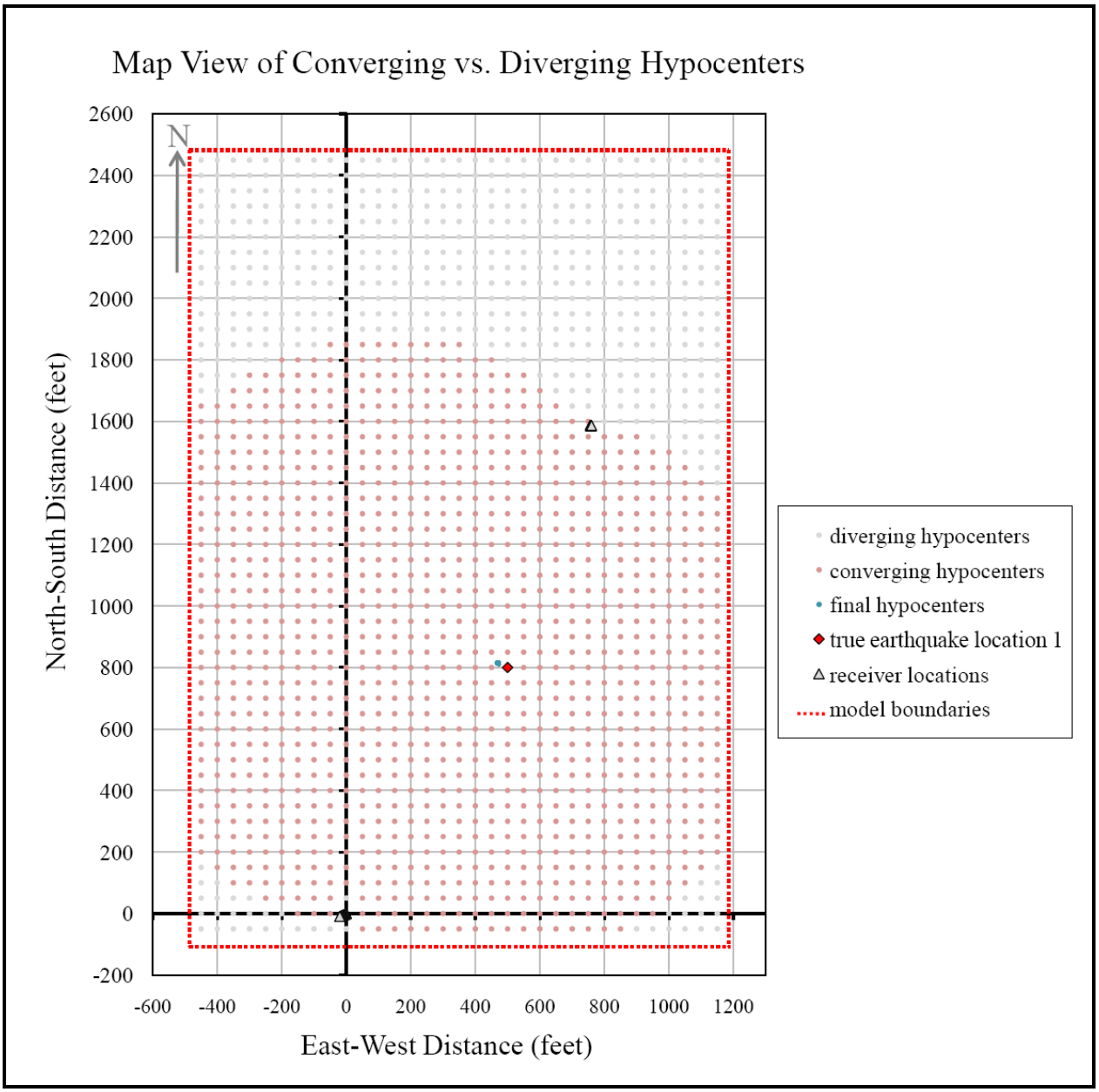

Figure 6.5: Map view of starting hypocenters that converge to the true earthquake location (pink) versus those that diverge in early iterations to positions outside of the model (gray). Final locations for the hypocenters that converge are shown in blue relative to the true earthquake location, represented by a red diamond. This ideal behavior of converging to the true location was observed for cases where the true earthquake location was close to the between-well line. These results are for true earthquake location 1, at spatial coordinates (500, 800, -8800).

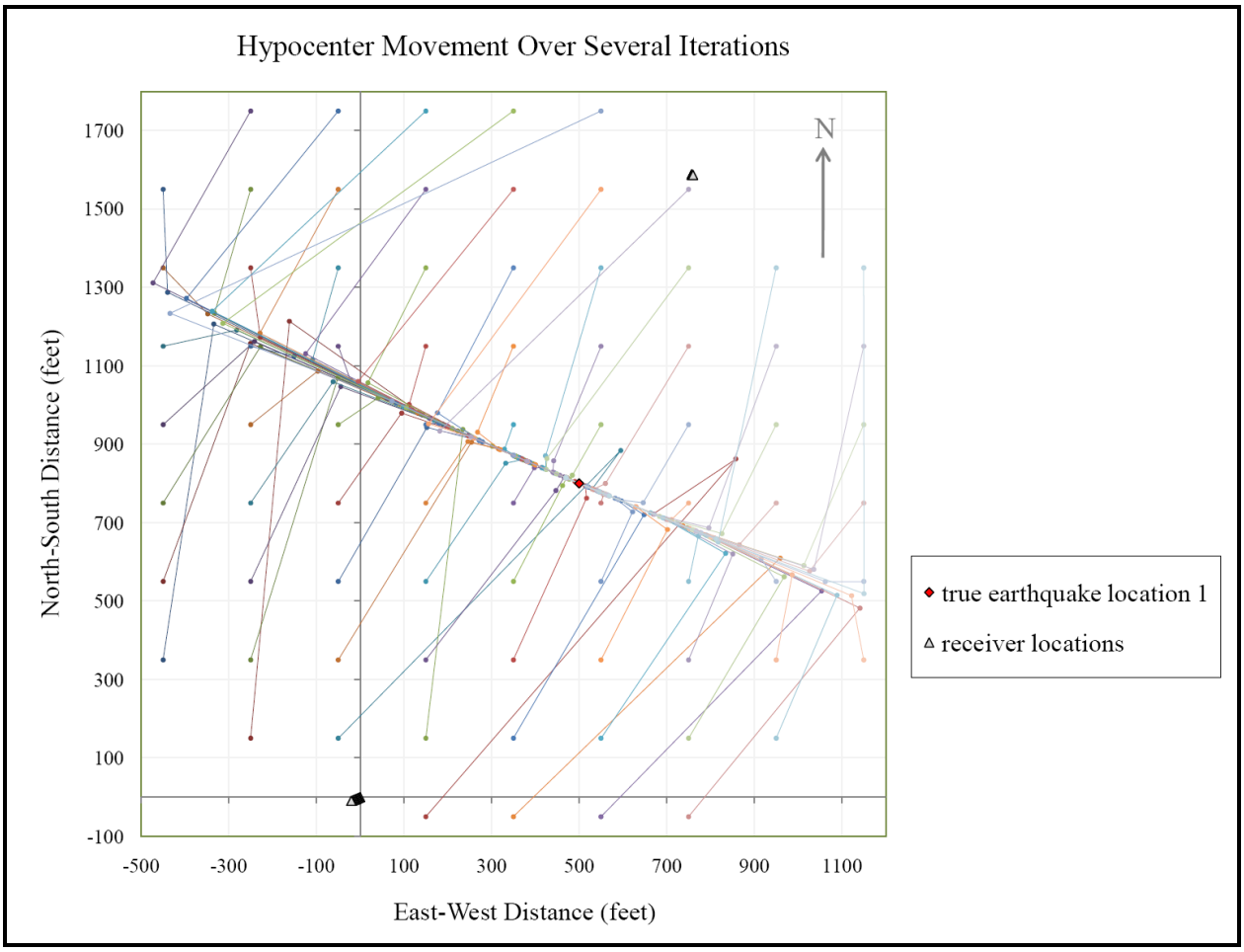

Figure 6.6: Convergence paths of hypocenters to true earthquake location over several iterations. For clarity, only hypocenters starting in the plane of the earthquake are displayed, at 200-ft spacing. These results are for true earthquake location 1, at spatial coordinates (500, 800, -8800).

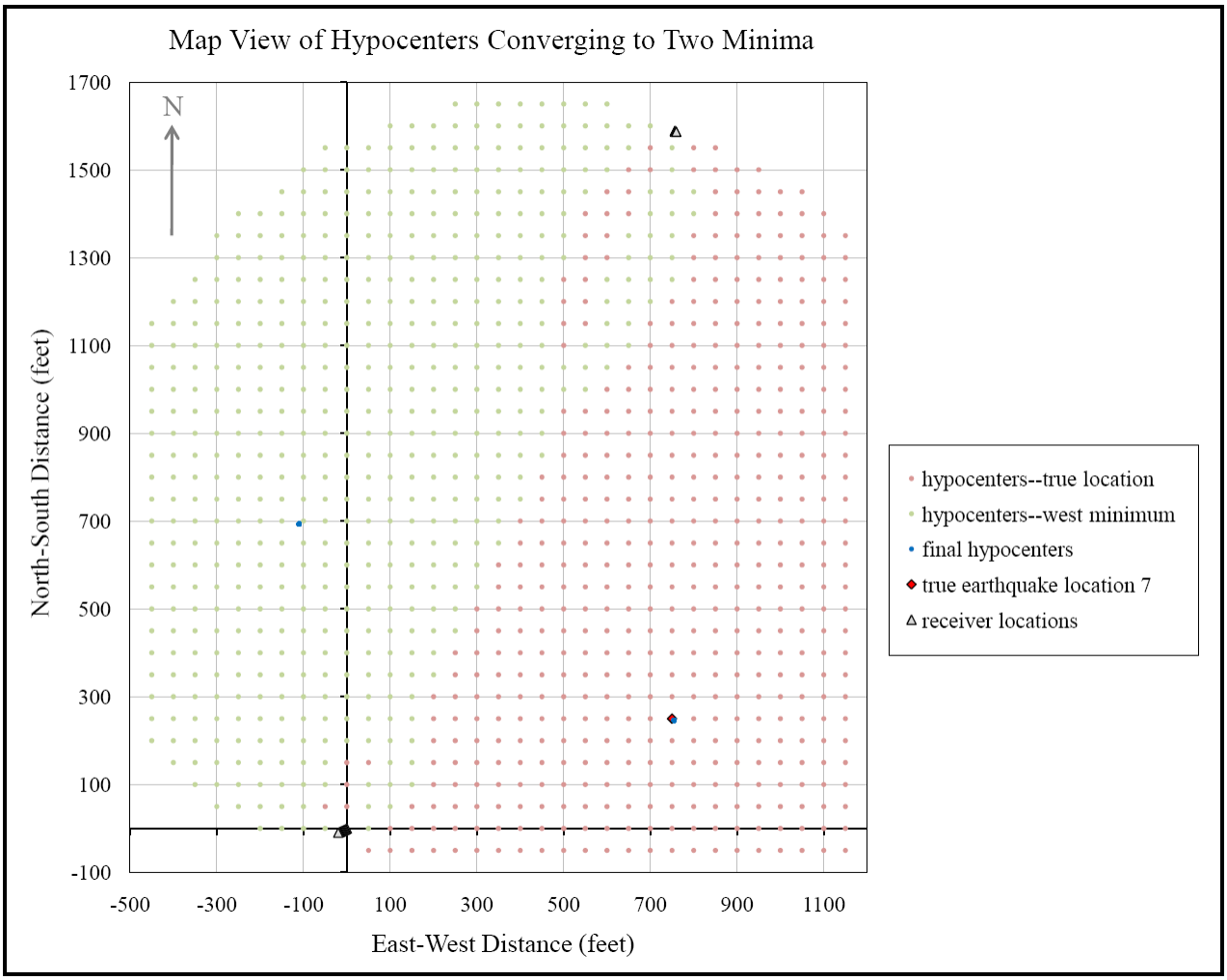

Figure 6.7: Map view of starting hypocenters that converge to the true earthquake location (pink) versus those that converge to the second minimum west of the between-well line (green). Starting hypocenters at the edge of the model (not shown) diverged to positions outside the model in early iterations. Final locations for the hypocenters that converge are shown in blue relative to the true earthquake location, represented by a red diamond. Convergence to two minima was observed for cases where the true earthquake location was a significant distance from the line between wells. These results are for true earthquake location 7, at spatial coordinates (750, 250, -8800).

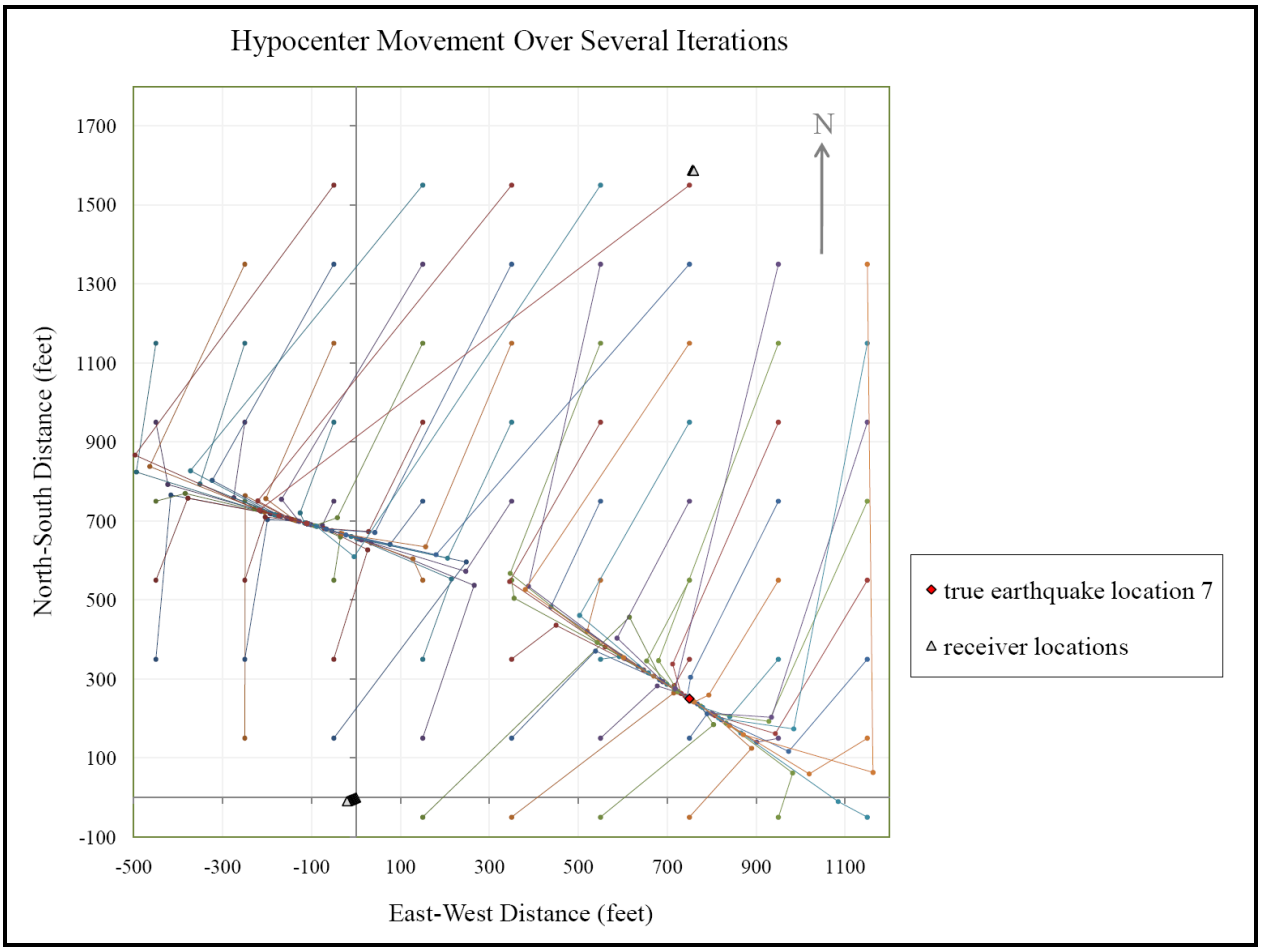

Figure 6.8: Convergence paths of hypocenters to true earthquake location and second minimum over several iterations. For clarity, only hypocenters starting in the plane of the earthquake are displayed, at 200-ft spacing. These results are for true earthquake location 7, at spatial coordinates (750, 250, -8800).

Investigation 3: Effect of Recording Geometry

Geometric location artifacts observed in Investigation 2 indicate a dependence upon recording geometry. Earthquakes that do not converge to the true location are pushed in the direction perpendicular to the between-well line toward a second minimum. This observation suggests that recording geometry fails to constrain specific directions, resulting in bias of the location. The one-well case has already been documented to lack azimuthal constraint (Rutledge et al., 2004). The azimuthal direction is constrained only by three-component ground motion. Adding a second observation well constrains the azimuth, but two error minima still exist along the line perpendicular to the line between wells. Adding a third observation well should improve geometric constraint and result in just one error minimum and a unique solution.

Three synthetic tests were conducted to assess the effect of recording geometry on location error. Each test incorporated different recording geometry. True earthquake locations were defined at 50-ft spacing throughout the model volume (Figure 3.7) and were the same for all tests. Starting hypocenters were the same as the true hypocenters. Error-free travel times were calculated through a constant velocity model for each recording geometry scenario. With this experiment design, the inversion is testing the ability of the recording geometry to determine the earthquake location, with no traveltime errors.

Test 1: Two Vertical Wells

The first test conducted used the two-well recording geometry of the real data set. Both receiver arrays are nearly vertical and located above the reservoir where fracturing is induced. Results of this test show that hypocenters are located an average of 7.3 feet from their true locations. This error seems reasonable for numerical effects considering the finite-difference

traveltime grid cell size of 10 feet. However, a significant number of hypocenters are mislocated by as much as 133.7 feet. Figure 7.1 is a map view slice of the final hypocenters at a depth of 9300 feet, within the reservoir depth range. Hypocenters close to the between-well line experience the largest location errors. The horizontal error is much larger than the vertical error; error is largest in the x-direction, followed by the y-direction, and finally the z-direction. Hypocenters within the vertical range of the receiver arrays experience less location error than those above or below, as shown in Figure 7.2. Here hypocenters are within the receiver range at a depth of 8800 feet, and although location error remains largest along the between-well line, the magnitude of error is reduced in all dimensions, and average error for all hypocenters at this depth is less than half that for hypocenters at 9300 feet. This result suggests that small numerical errors may cause relatively large hypocenter mislocations for this recording geometry. The location error for earthquakes directly between the wells is in the direction perpendicular to the raypaths from the earthquakes to the receiver stations. A small change in hypocenter location in this direction has very little effect on the observed travel times.

Test 2: One Vertical Well and One Horizontal Well

Altering the recording geometry so that one of the wells and its array of receivers are horizontal rather than vertical should better constrain hypocenters in the horizontal dimension. The receiver stations associated with the Lowery #3 well were redefined in a horizontal configuration (Figure 7.3) to simulate results from a horizontally-drilled observation well. The original receiver spacing from Lowery #3 was maintained, but receivers were oriented along a line perpendicular to the line between real wells, at a depth of 8885.9 feet, the average receiver

depth from Lowery #3. In a realistic scenario, a horizontal well in a survey area is likely to be within the reservoir, providing an optimal version of this geometry.

Inversion of the error-free synthetic data with this recording geometry produces a strong improvement in the hypocenter locations. The location error is too small to be detected visually at the scale of Figure 7.4 because these hypocenters are surrounded by the recording geometry in all dimensions. On average, the hypocenters locate only 3.2 feet from their true locations; this is less than half the average error produced using two vertical wells. The maximum error on hypocenters is also reduced by more than half, to 65.4 feet. Horizontal errors are reduced and are similar to vertical errors for this recording geometry. The average error for all hypocenters is greatest in the y-direction, which could be inferred from the orientation of the horizontal receivers, which better constrains the x-direction. For the hypocenters at 9300 feet (Figure 7.4), errors are largest in the z-direction, perhaps because these hypocenters are below the depth range of the receivers, which is reduced by the reorientation of the Lowery #3 well. The z-direction is the best constrained direction for hypocenters at 8800 feet, within the depth range of the receivers.

Test 3: Three Vertical Wells

An alternate way to improve the poor performance of the two-vertical-well recording geometry is to add a third vertical well. This improvement may be more practical than using a horizontal observation well, as horizontal wells are typically used for production or fracture treatments, making them less likely to be available. The three-well recording geometry was tested by defining a third well at a considerable horizontal distance from the other two, as shown in Figure 7.5. The depth range and spacing for the receiver array are averages of the other wells.

This recording geometry produces the best location results of all those tested. The average location error is less than 2 feet and maximum error is 13.5 feet, approximately one-fifth of the maximum error from Test 2 and one-tenth of the error from Test 1. Errors are reduced in all spatial directions. Examination of hypocenters at a depth slice of 9300 feet reveals that the z-direction is the least constrained, but it is better than any of the previous results. The plotted hypocenters appear the same as starting hypocenters in Figure 3.7, as errors are too small to plot. For a depth slice at 8800 feet, where a central earthquake cluster would be surrounded by receivers in all directions, hypocenters show the least error, with average error less than 1 foot in all directions. Errors for this depth slice are also too small to plot. This recording geometry is more expensive but significantly improves the accuracy of hypocenter locations.

Figures

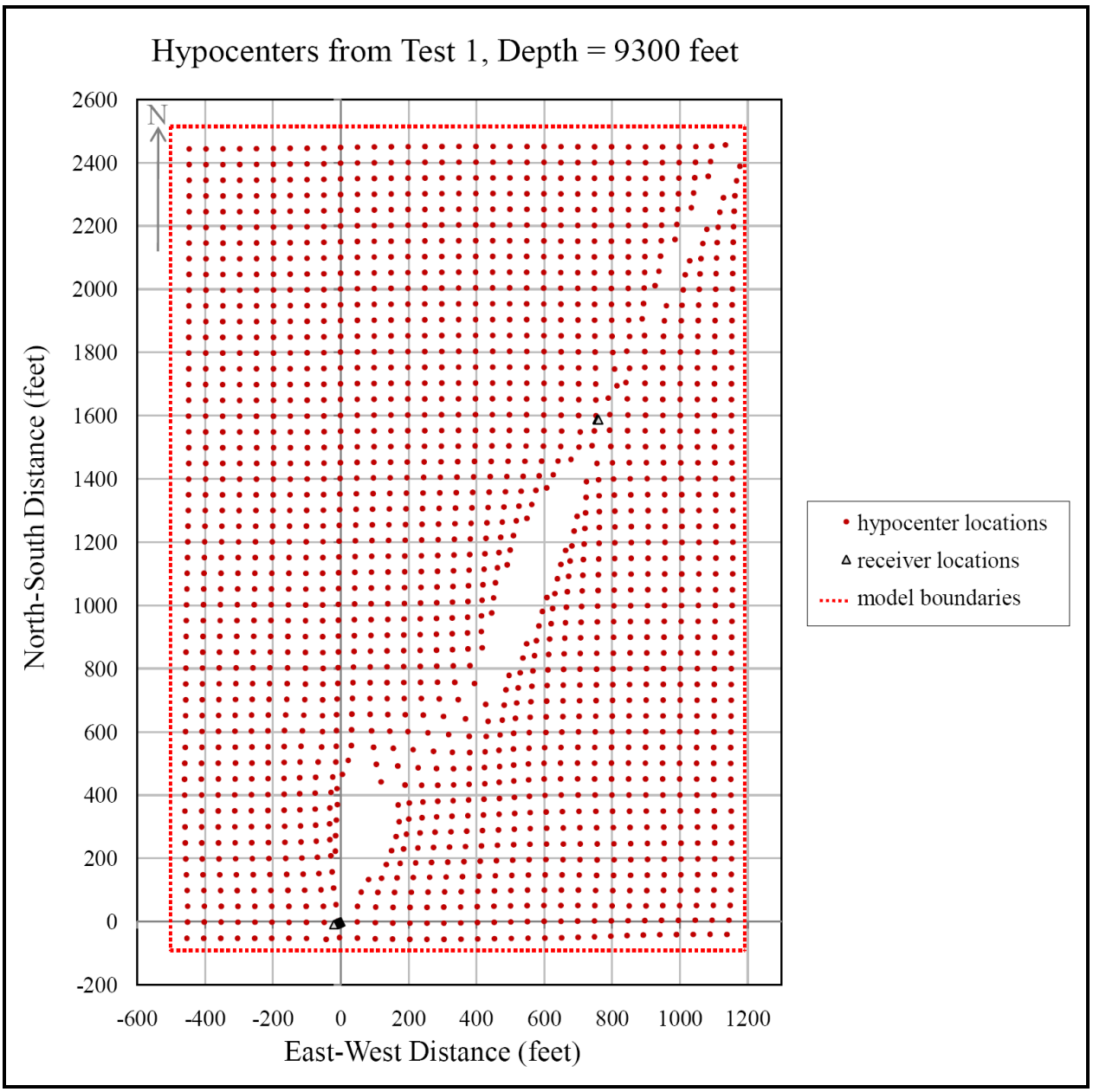

Figure 7.1: Depth slice of relocated hypocenters at 9300 feet for Test 1 (two vertical wells). Depth is within the reservoir depth range and below the receiver depth range. Location error is greatest for hypocenters near the line between wells.

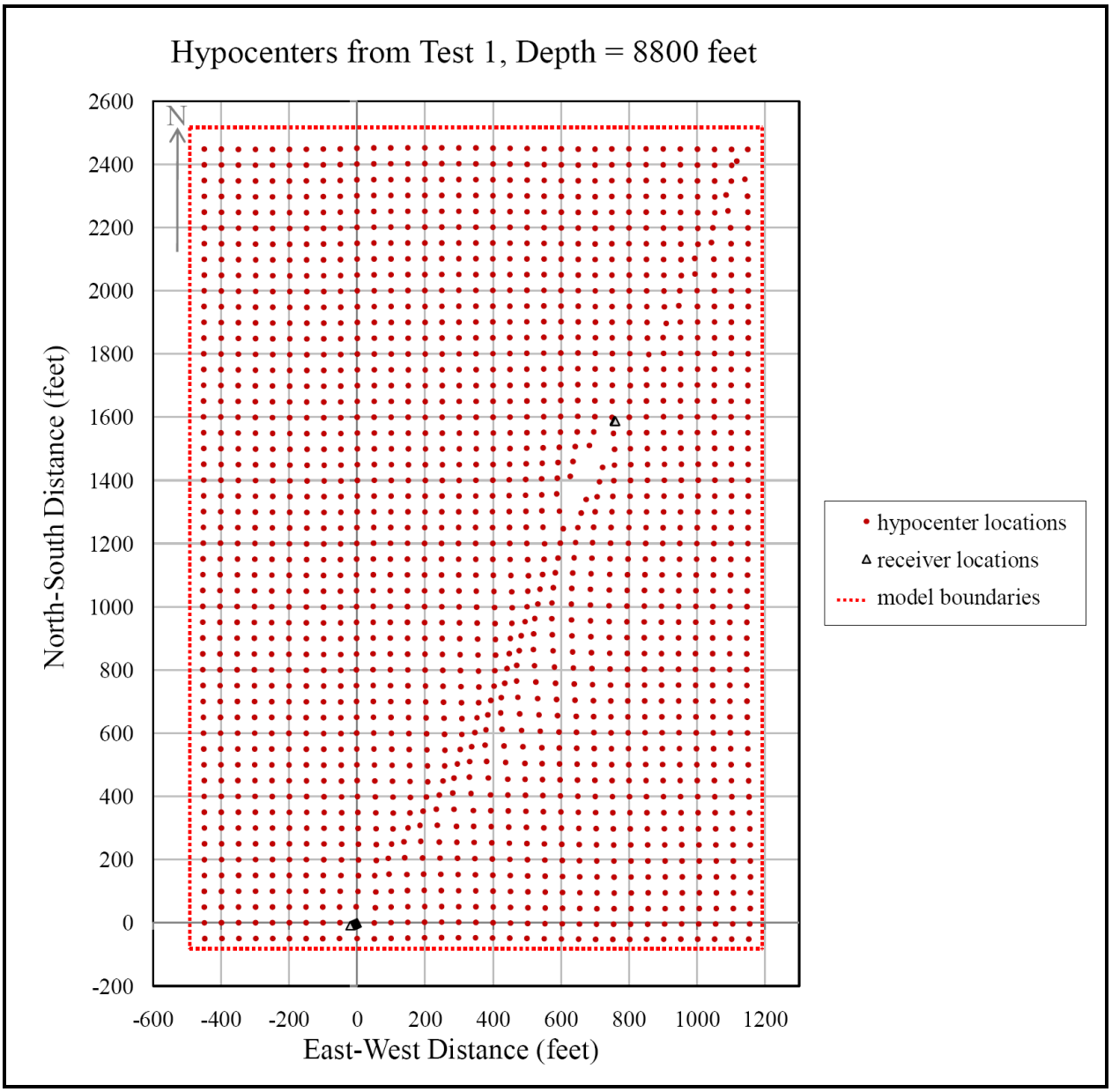

Figure 7.2: Depth slice of relocated hypocenters at 8800 feet for Test 1 (two vertical wells). Depth is above the reservoir depth range and within the receiver depth range. Location error is much less than for hypocenters at 9300 feet (Figure 7.1) but is still greatest for hypocenters near the line between wells.

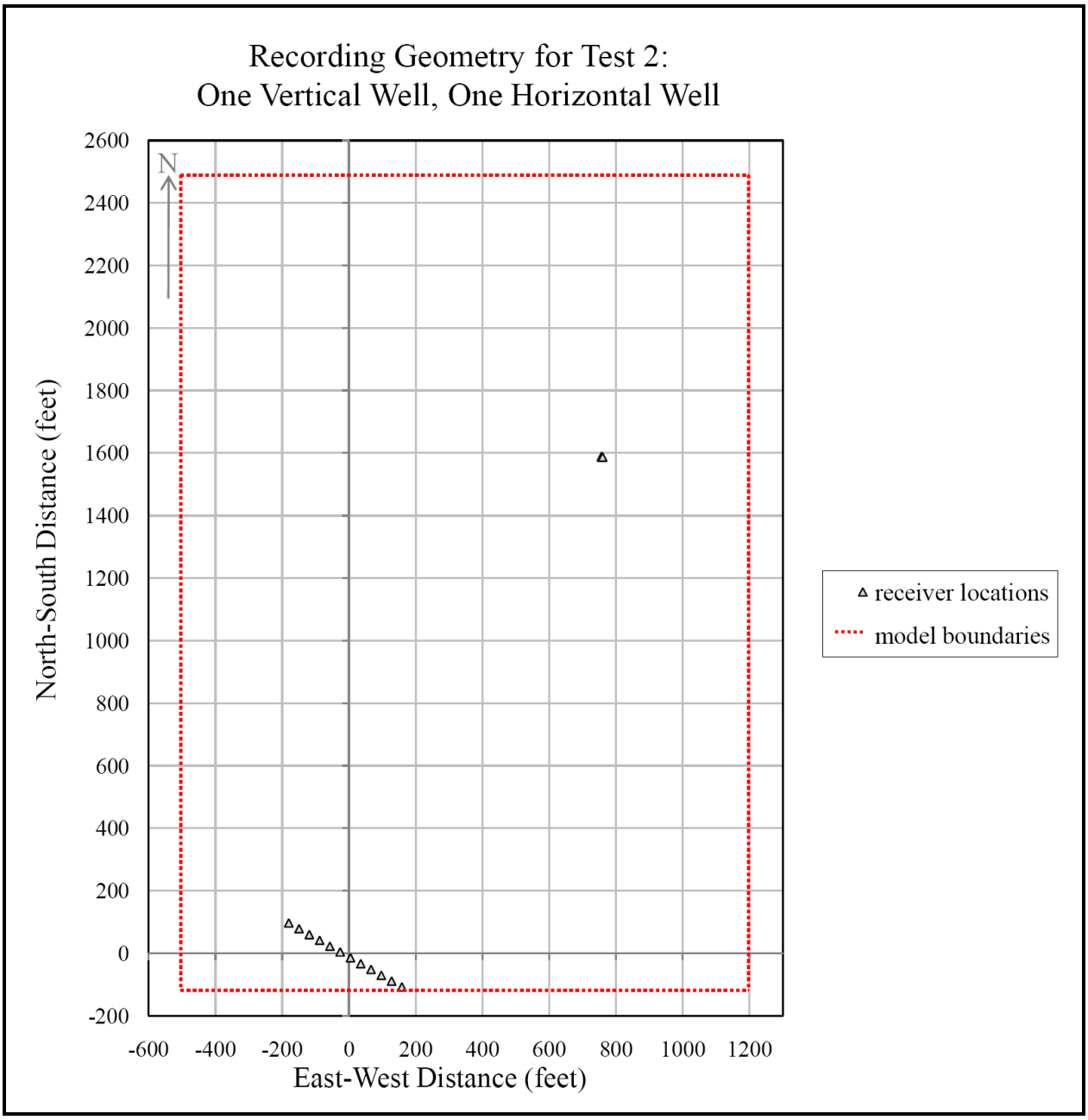

Figure 7.3: Map view of recording geometry for Test 2 (one vertical well, one horizontal well). The southwest vertical well from the real survey geometry (Lowery #3) has been replaced with a horizontal well, perpendicular to the between-well line, at the average depth of the real array.

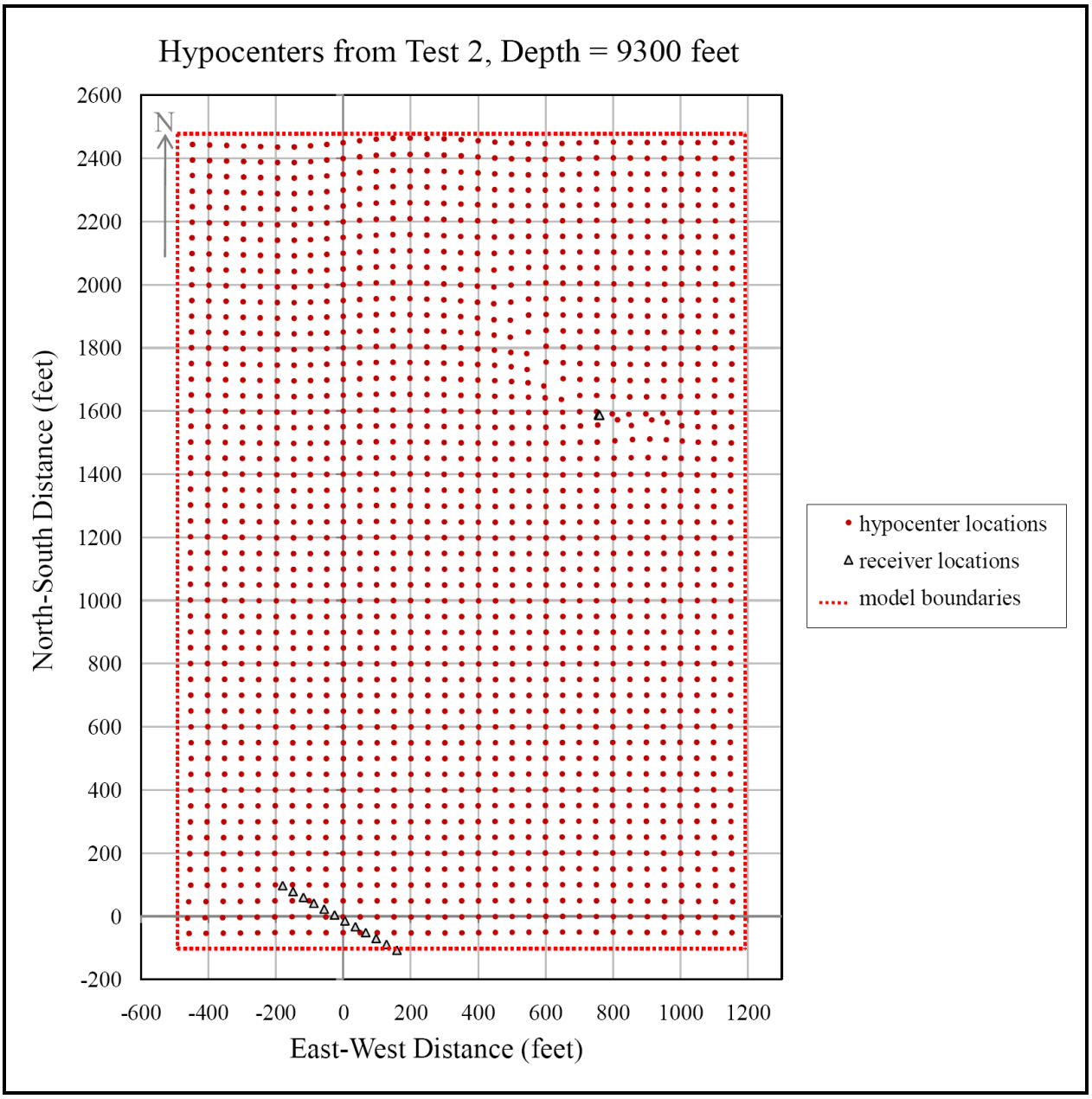

Figure 7.4: Depth slice of relocated hypocenters at 9300 feet for Test 2 (one vertical well, one horizontal well). Depth is within the reservoir depth range and below the receiver depth range. Location errors are greatly reduced, demonstrating the improved horizontal constraint of this recording geometry.

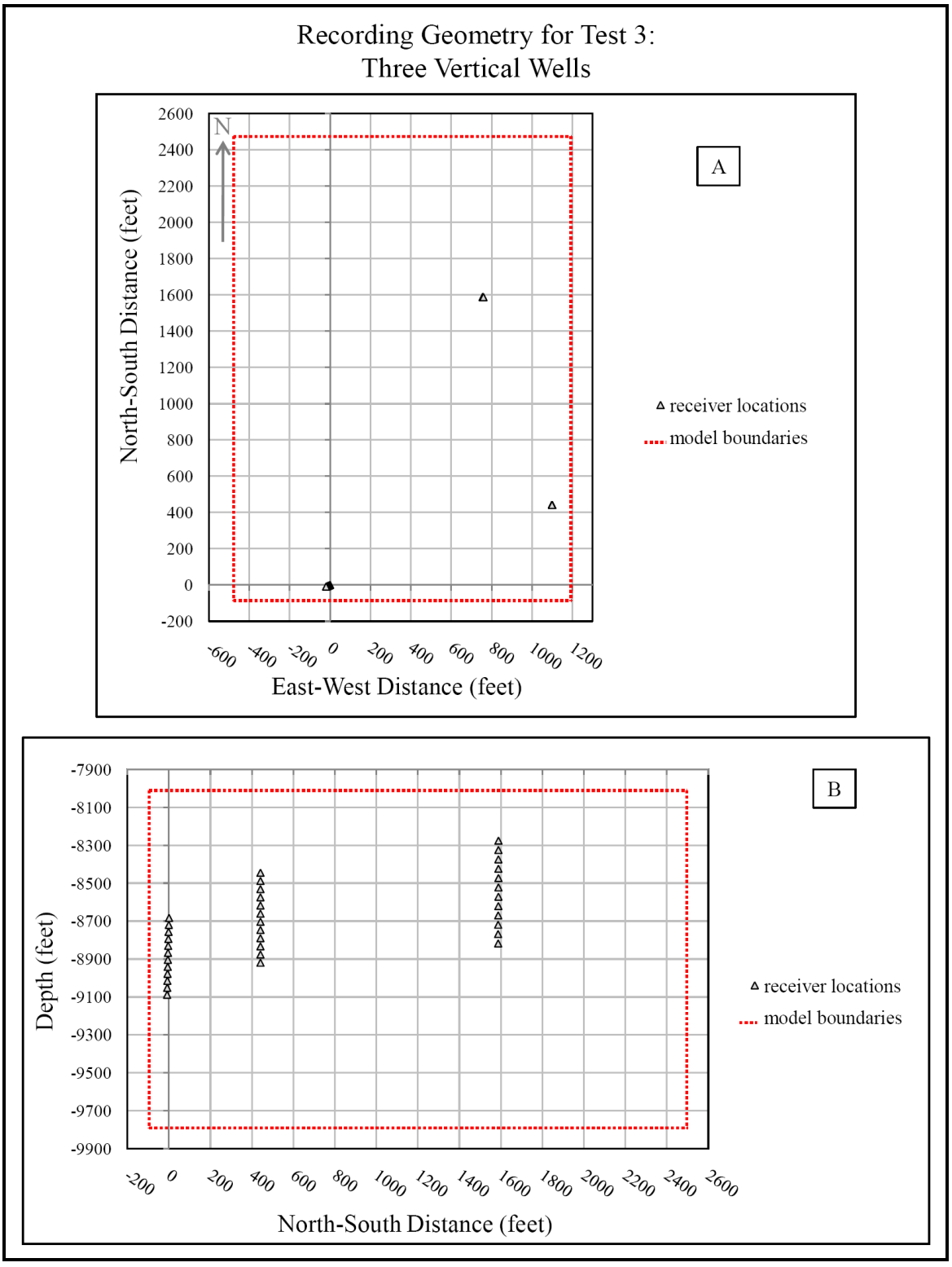

Figure 7.5: Recording geometry for Test 3 (three vertical wells) in map view (A) and North-South cross section (B). A third well of receiver stations is added at considerable lateral distance from the other two. Similar receiver spacing and depth range for receivers are maintained.

Investigation 4: Effect of Picking Error

The seismic records have low signal-to-noise ratios, particularly for P-waves, creating significant uncertainty in the arrival time picks. A low level of signal relative to noise is a destabilizing factor in iterative inversion methods and an obstacle in tomographic imaging (Phillips and Fehler, 1991). Because of the low P-wave signal amplitudes, only S-wave arrival time picks could be used in the inversion of the real data. The lack of P-wave arrival time data causes the tradeoff between earthquake time and distance to be poorly constrained. The uncertainty in arrival times, combined with limited geometrical constraint, has a large effect on the final hypocenter locations. Tests were conducted using both real and synthetic data sets to investigate the effect of picking errors on the hypocenter location error.

Real Data Test

The quality of arrival time picks was evaluated for a representative subset of the seismic records to explore a possible connection between the quality of arrival time picks for an earthquake and the ability to locate the hypocenter. Quality categories A, B, C, and X were assigned by considering factors including signal-to-noise, the number of traces picked, and the behavior of the arrival-time move-out curve defined by those picks (Figure 8.1). Category A was assigned to the highest quality picks and had an average estimated picking error of 2.1 milliseconds. Category B picks were of lower quality and had an average estimated picking error of 2.9 milliseconds. Category C was assigned to the lowest quality picks and had an average estimated picking error of 4.6 milliseconds. Category X was reserved for arrivals that could not be reliably detected. Pick quality was assessed separately for P-wave and S-wave

arrivals and for receiver arrays for the two wells, so that for each record, four quality factors were obtained (Table 8.1, Figure 8.2).

The P-wave arrivals have lower signal strength than the S-arrivals and, therefore, have lower quality picks. The Lowery #3 well has a large number of unpickable (X-quality) P-wave arrivals due to the large distance between the well and the location of stage 3, where most of the earthquakes in the data set occur. The lack of P-wave picks for one well prompted the use of only S-waves for this study, whose goal is an exploration of the advantages and utility of two wells over a single well. It was anticipated that the accuracy of the arrival time picks should correlate with the poor performance of the S-wave real data hypocenter results of the original inversion attempt.

Three subsets of earthquakes were examined for possible trends through several iterations of the inversion. For each subset, the S-wave picks on both wells were of equal quality, such that one subset contained all earthquakes of entirely A-quality picks, one contained all earthquakes of entirely B-quality picks, and one contained all earthquakes of entirely C-quality picks. No systematic improvement of the SeisPT starting hypocenters (Figure 8.3) or final hypocenters (Figure 8.4) was detected for picks of better quality. The percentage of earthquakes retained after 60 iterations of the damped inversion was roughly equal: 44%, 43%, and 47% for A, B, and C quality, respectively. The rates at which hypocenters diverged from the model during the iterative inversion were similar for all subsets. With many factors contributing to hypocenter location errors on the real data, a relationship between picking error and location error may be disguised by other contributing factors.

Synthetic Data Test

A study using synthetic data was designed to test the effect of realistic picking error on hypocenter locations when all other input data are error-free. The eight hypocenters defined as true earthquake locations for the synthetic data test in Investigation 2 (Figure 6.4) were used again in this investigation. The true locations were also used as starting hypocenters. Error-free arrival-time picks were calculated for all receivers. Random errors based on picking error estimates from the real data were then added to the true picks. Random errors were drawn from a normal distribution with zero mean and standard deviation of 2.9 milliseconds, similar to B-quality picks. For each earthquake, one hundred sets of random errors were generated and added to the true arrival times for one hundred separate inversions. This produced a cluster of hypocenters for different random errors for the same earthquake.

The final hypocenters contain large location errors that average 270.8 feet from their true locations with a maximum location error of 1318.6 feet. Location errors are largest in the x-direction, followed by y- and z- directions at a ratio of approximately 5: 2.5: 1. Examination of the hypocenters in map view (Figure 8.5) shows that the large horizontal errors occur along the direction approximately perpendicular to the between-well line. In East-West and North-South cross sections (Figures 8.6 and 8.7), a relationship between earthquake depth and convergence behavior is revealed. Shallow earthquakes within the depth range of the receivers are well constrained in depth, while those below the receiver range migrate significant distances in depth along a hyperbolic path.

A comparison of final hypocenters from the real and synthetic tests shows similarities in map view (Figure 8.8). Both sets of hypocenters display geometric scatter in the direction perpendicular to the between-well line and both extend similar distances (~2000 feet) along that line. From this comparison, the synthetic result appears to model the real data result. However,

the real data earthquakes may be aligning with fracture geometry, whose orientation is similar to the direction of geometric scatter observed in both results. This possibility complicates any comparison of the results or conclusions about the origin of their similarities.

Figures

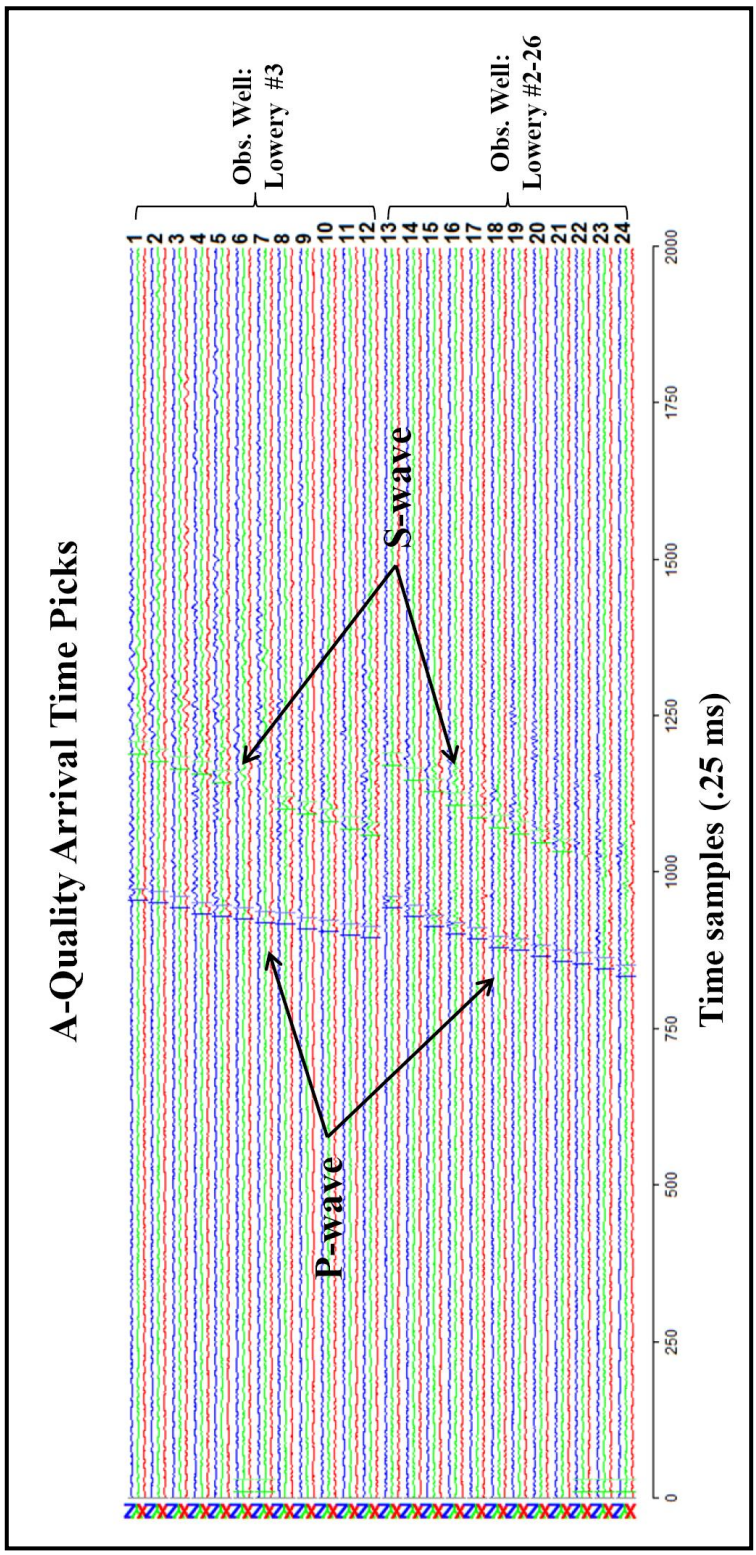

Figure 8.1 (A): Seismic record showing A-quality picks. A single event is present in this record. P-wave arrival picks are in blue and S-wave arrival picks are in green. Note that signal-to-noise is better than in records (B) and (C), all four arrivals are picked, most traces are picked for each arrival, and picks define a smooth curve.

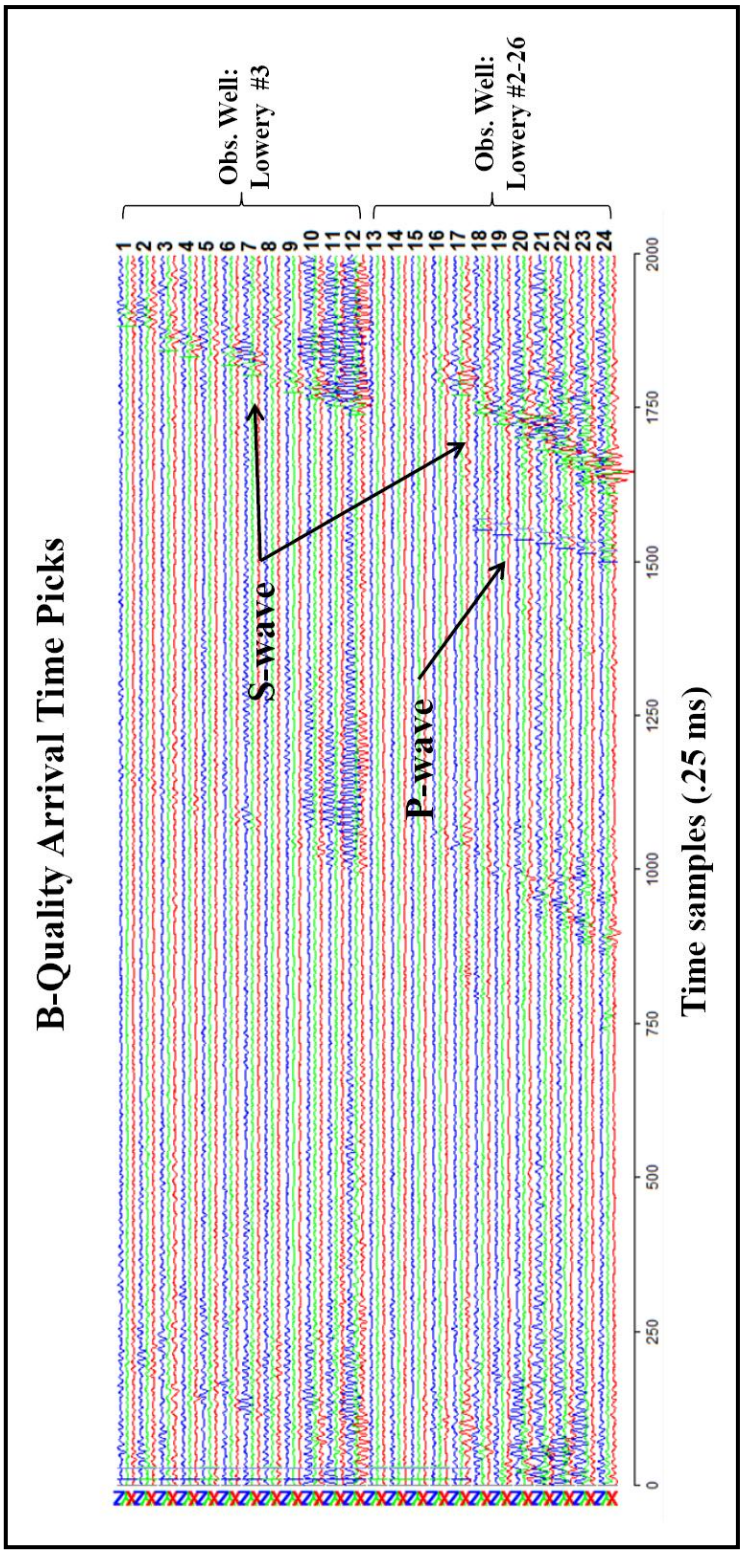

Figure 8.1 (B): Seismic record showing B-quality picks. Three events are present in this record, but picks are made only for the latest event. P-wave arrival picks are in blue and S-wave arrival picks are in green. Note that more noise is present than in record (A), the P-wave arrival is not picked for the first receiver array, and fewer traces are picked for each arrival.

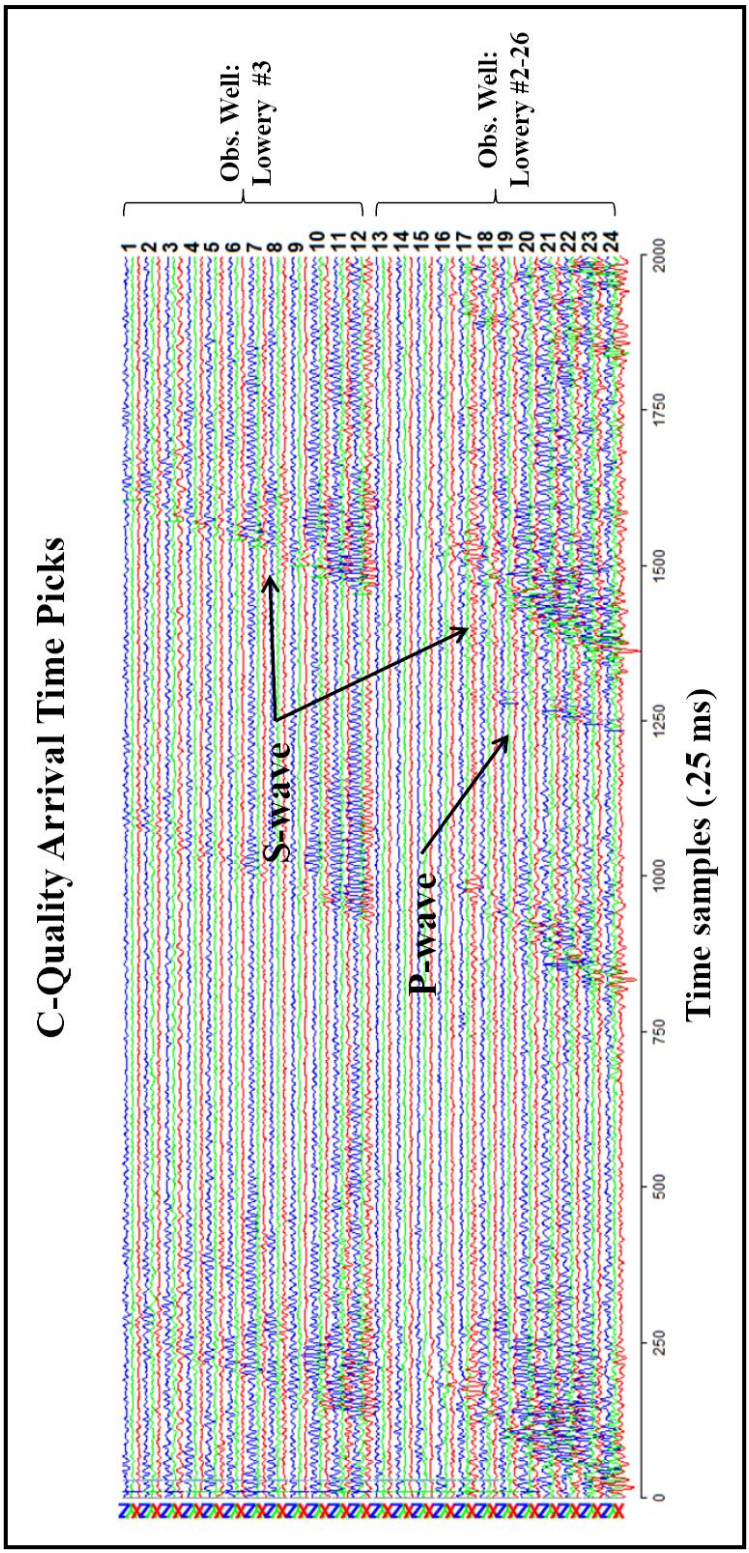

Figure 8.1 (C): Seismic record showing C-quality picks. Three events are present in this record, but picks are made only for the latest event. P-wave arrival picks are in blue and S-wave arrival picks are in green. Note that the noise is the highest of all records, the P-wave arrival is not picked for the first receiver array, few traces are picked for each arrival, and picks do not define smooth arrival curves.

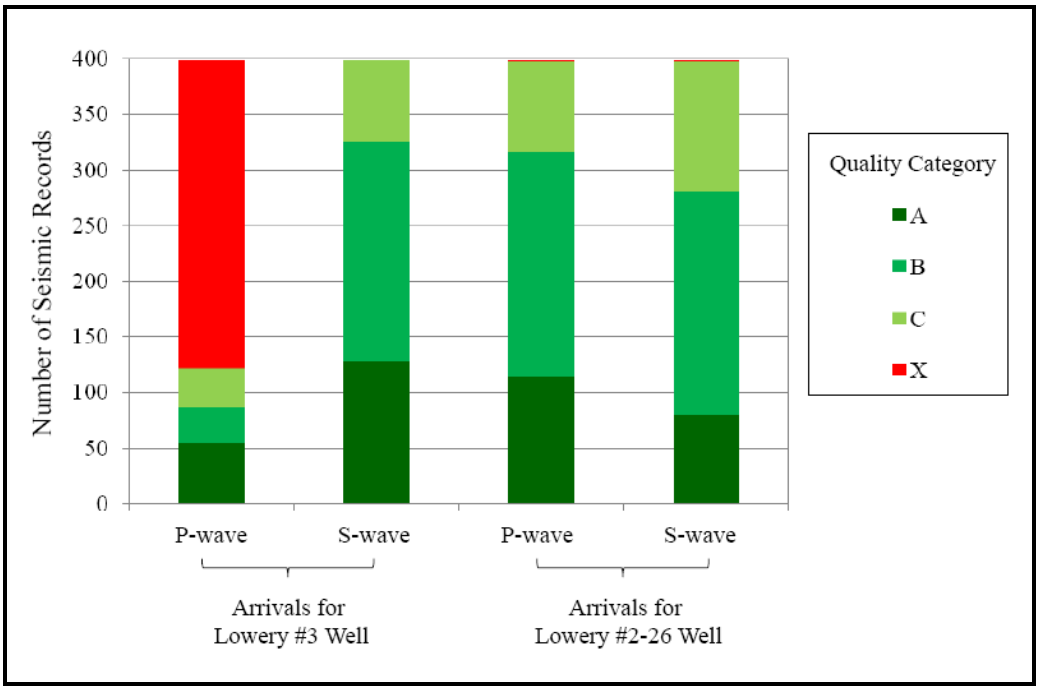

Figure 8.2: Relative picking quality for each of the four arrivals assessed (P-wave and S-wave for receiver arrays at each observation well). Picking quality is represented as the number records for which each arrival was assigned each quality category. Note the high number of X-quality picks for P-wave arrivals on the Lowery #3 well, illustrating the lack of P-wave data available to incorporate in the inversion.

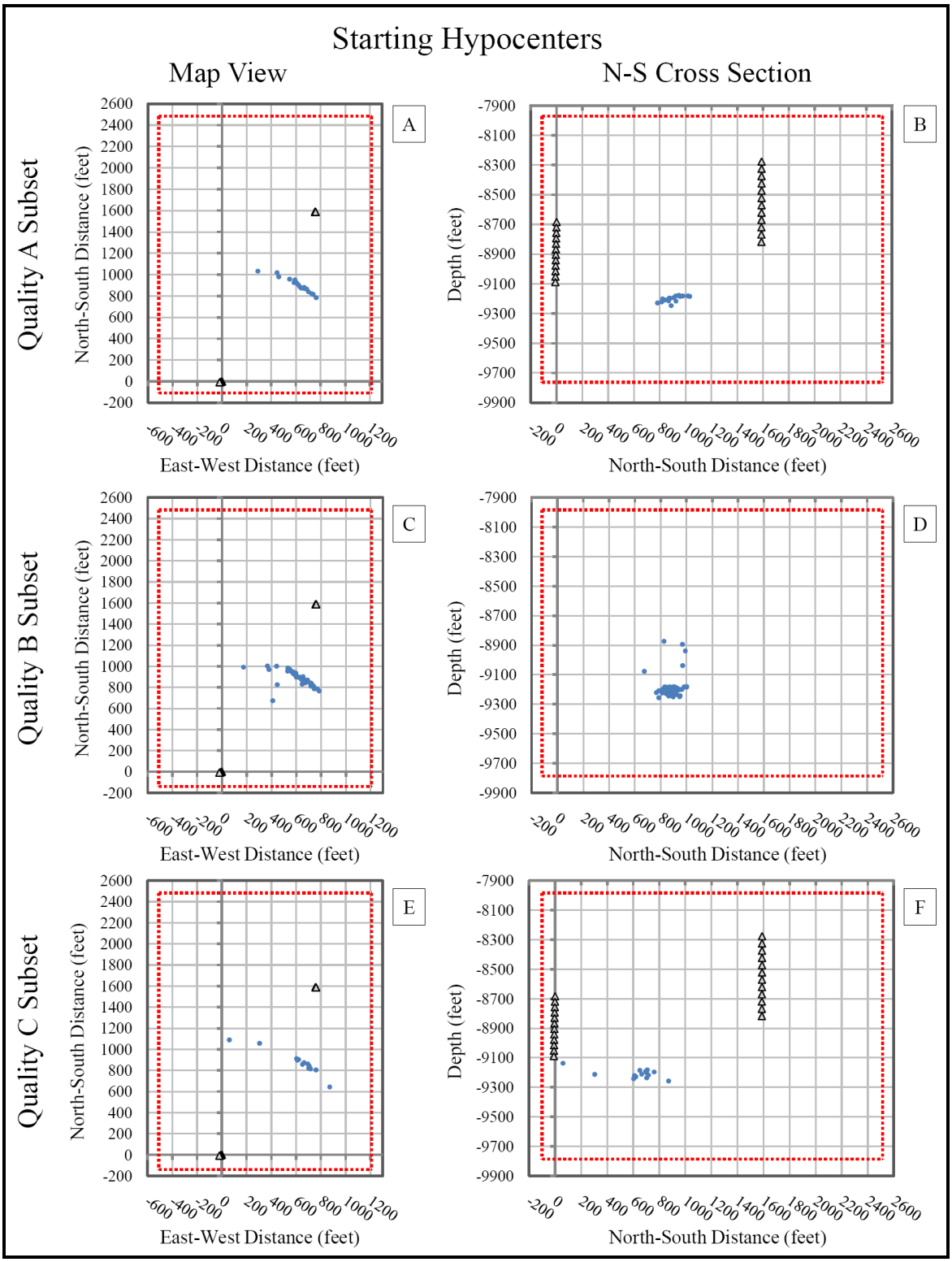

Figure 8.3: Starting hypocenters for A-quality picks in map view (A) and N-S cross section (B), B-quality picks in map view (C) and N-S cross section (D), and C-quality picks in map view (E) and N-S cross section (F). Receiver stations are represented by gray triangles. The red box is the model volume.

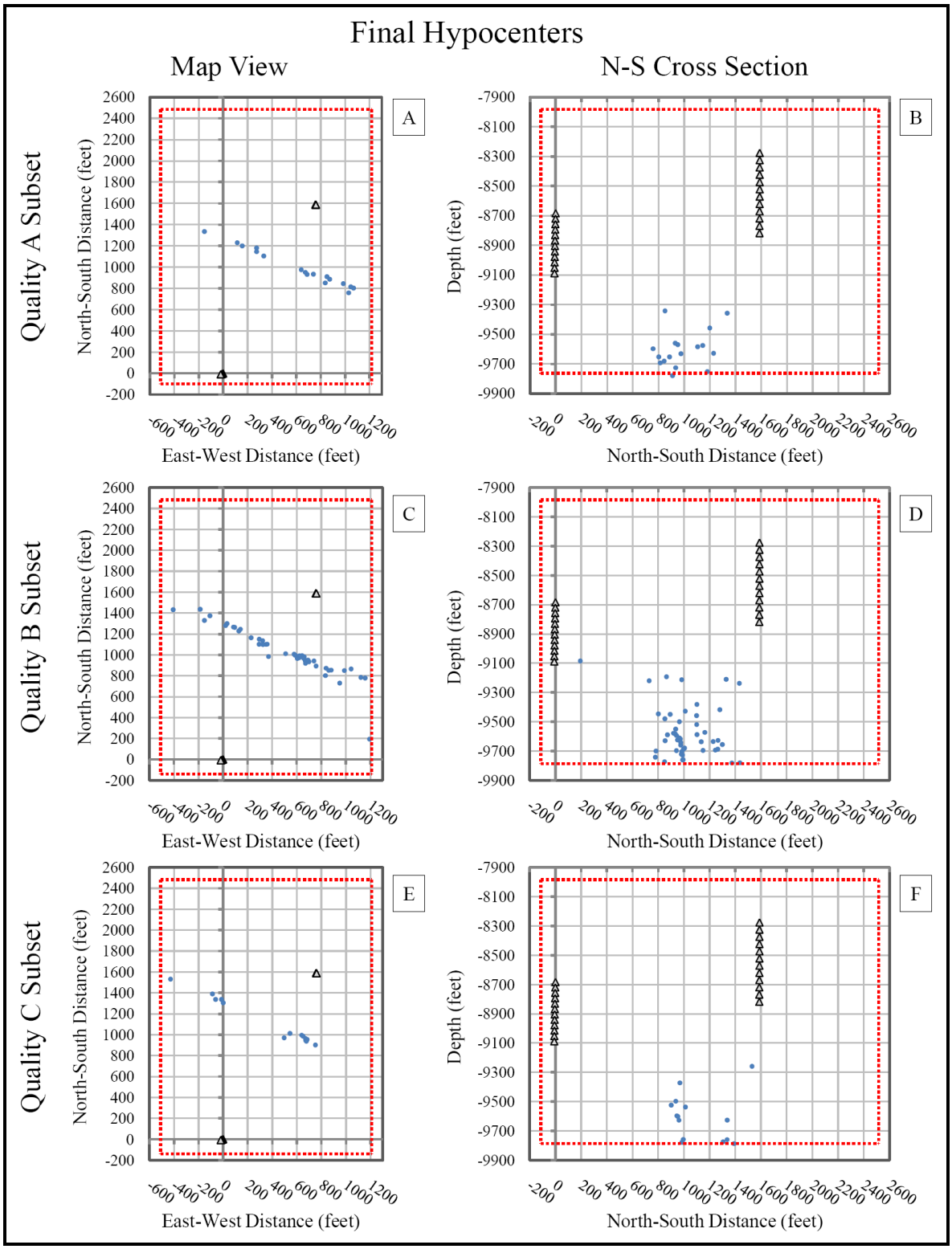

Figure 8.4: Final hypocenters for A-quality picks in map view (A) and N-S cross section (B), B-quality picks in map view (C) and N-S cross section (D), and C-quality picks in map view (E) and N-S cross section (F). Receiver stations are represented by gray triangles. The red box is the model volume.

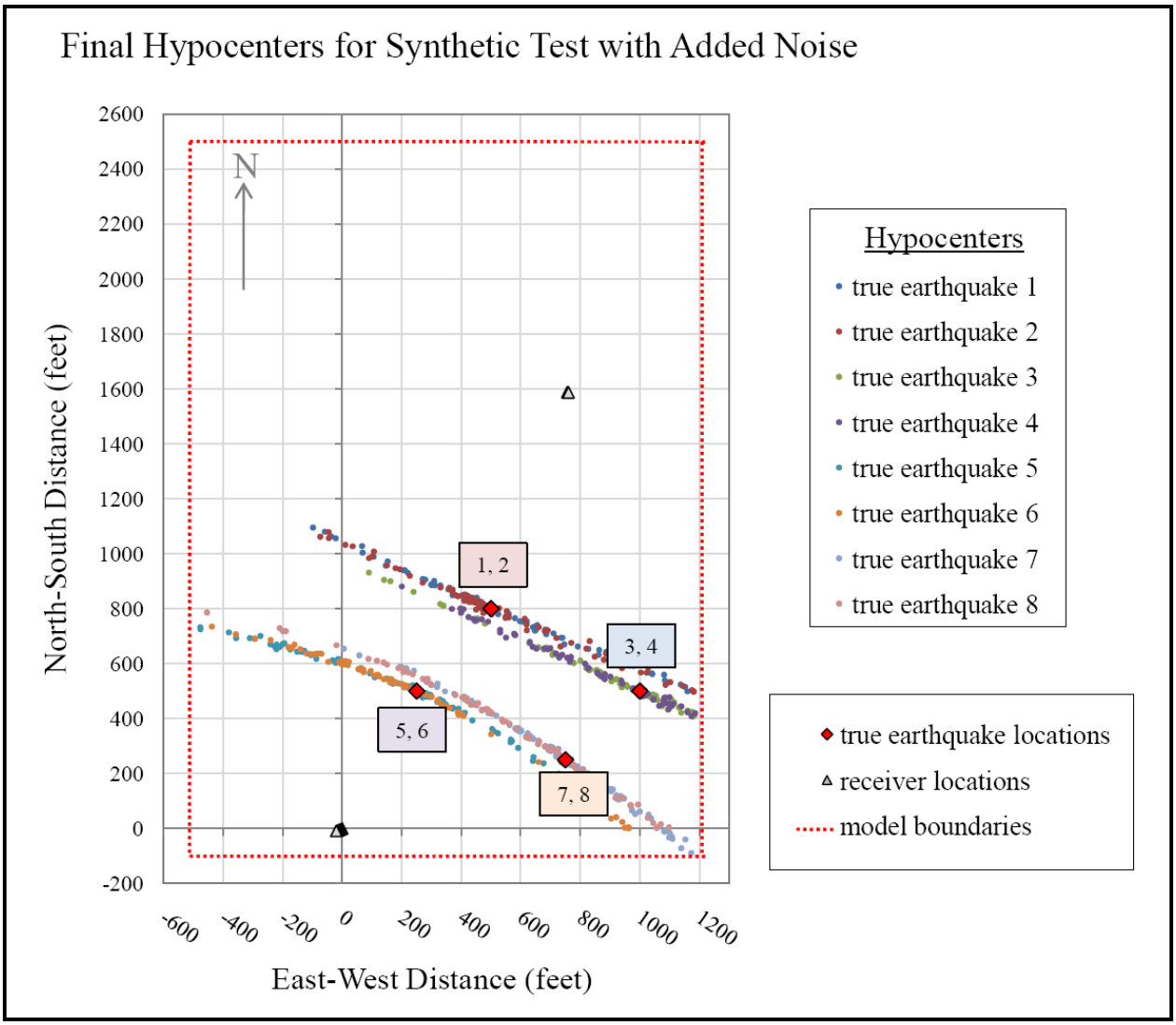

Figure 8.5: Map view of final hypocenters for noisy synthetic data showing large horizontal error in the direction perpendicular to the between-well line. Hypocenters for the same true earthquake location are displayed as points of the same color. True earthquake locations are represented by red diamonds; for spatial coordinates [X, Y, Z] of true earthquake locations, refer to Figure 6.4. Receiver stations are represented by gray triangles.

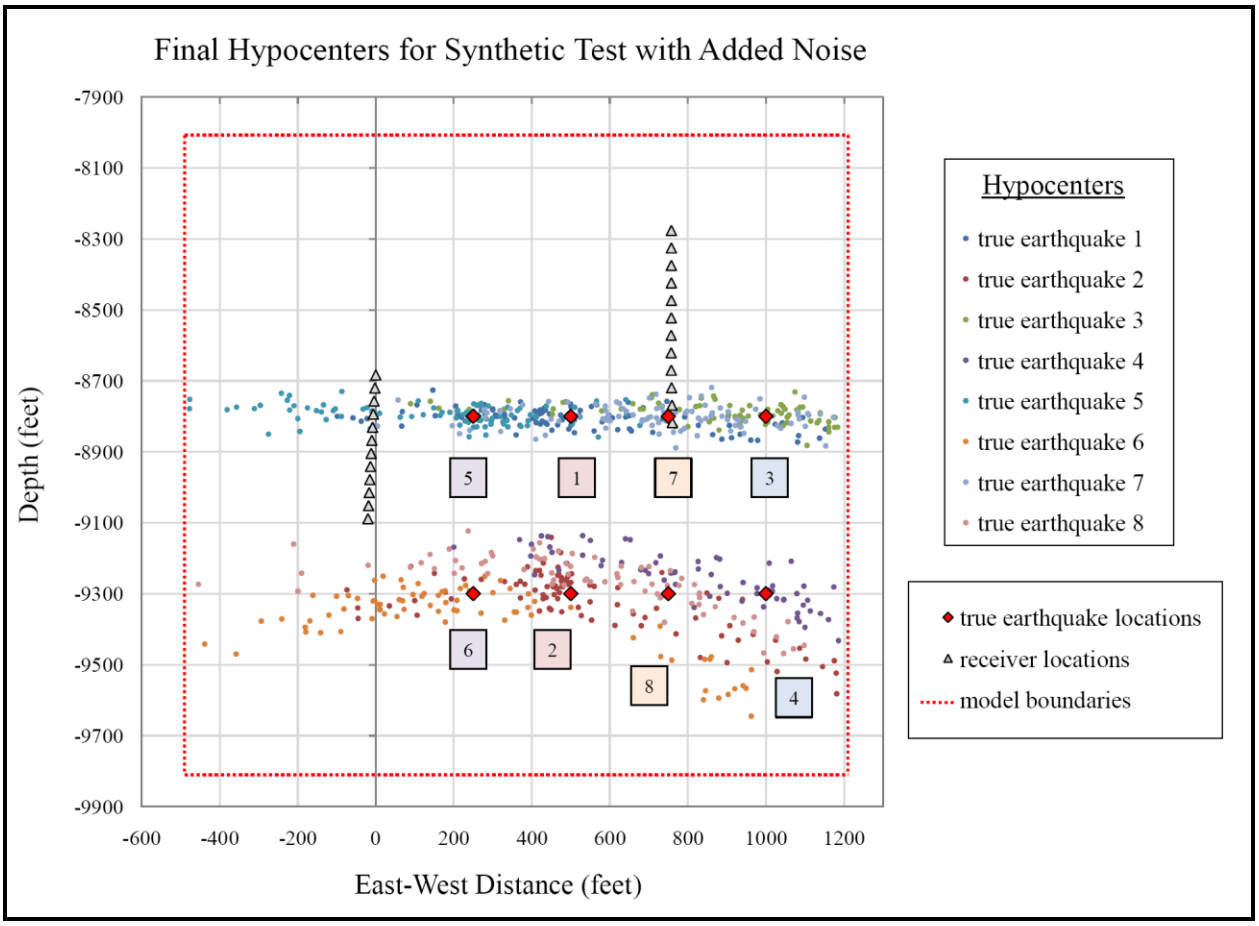

Figure 8.6: Final hypocenters for noisy synthetic data in East-West cross section. Hypocenters for the same true earthquake location are displayed as points of the same color. True earthquake locations are represented by red diamonds; for spatial coordinates [X, Y, Z] of true earthquake locations, refer to Figure 6.4. Receiver stations are represented by gray triangles.

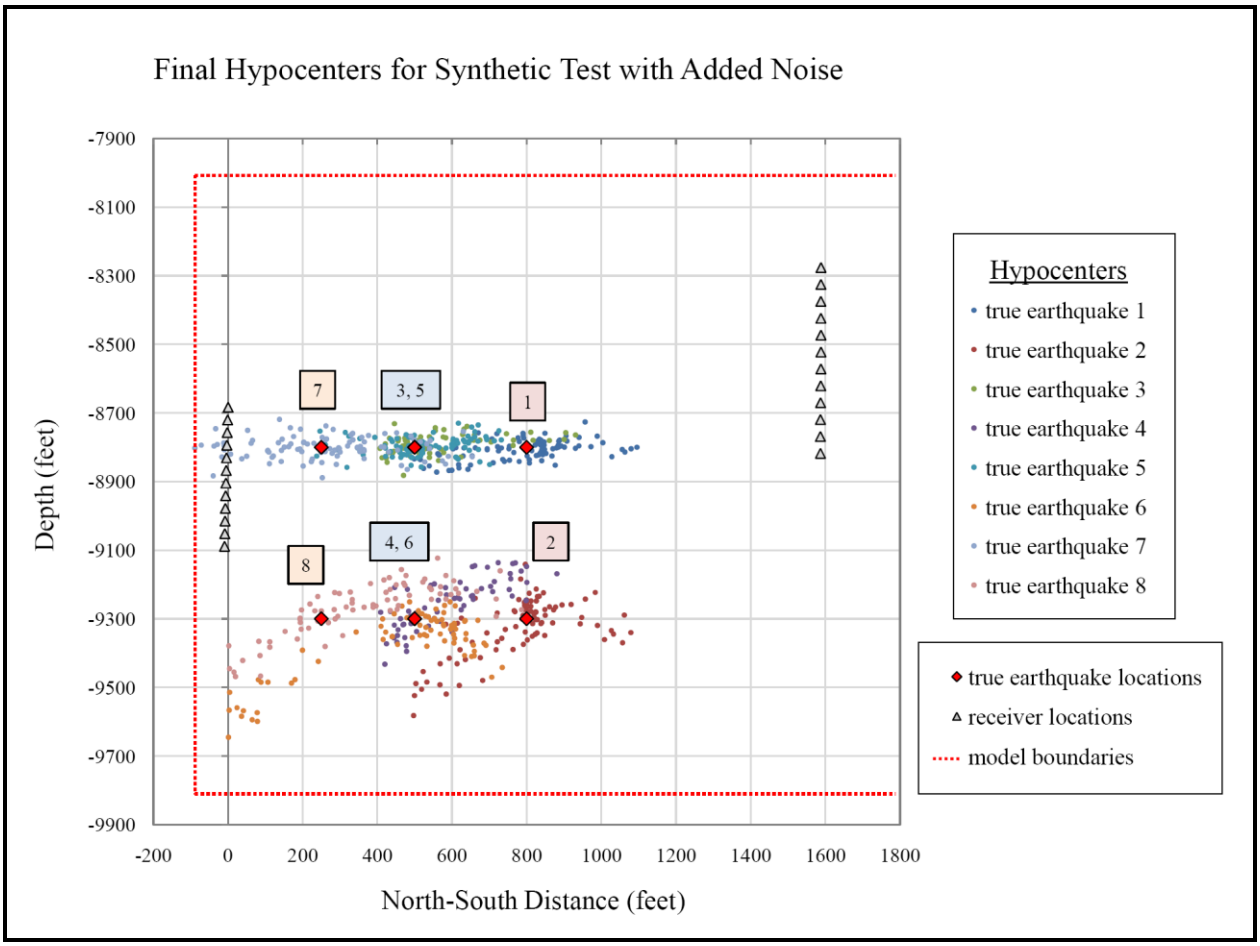

Figure 8.7: Final hypocenters for noisy synthetic data in North-South cross section. Hypocenters for the same true earthquake location are displayed as points of the same color. True earthquake locations are represented by red diamonds; for spatial coordinates [X, Y, Z] of true earthquake locations, refer to Figure 6.4. Receiver stations are represented by gray triangles.

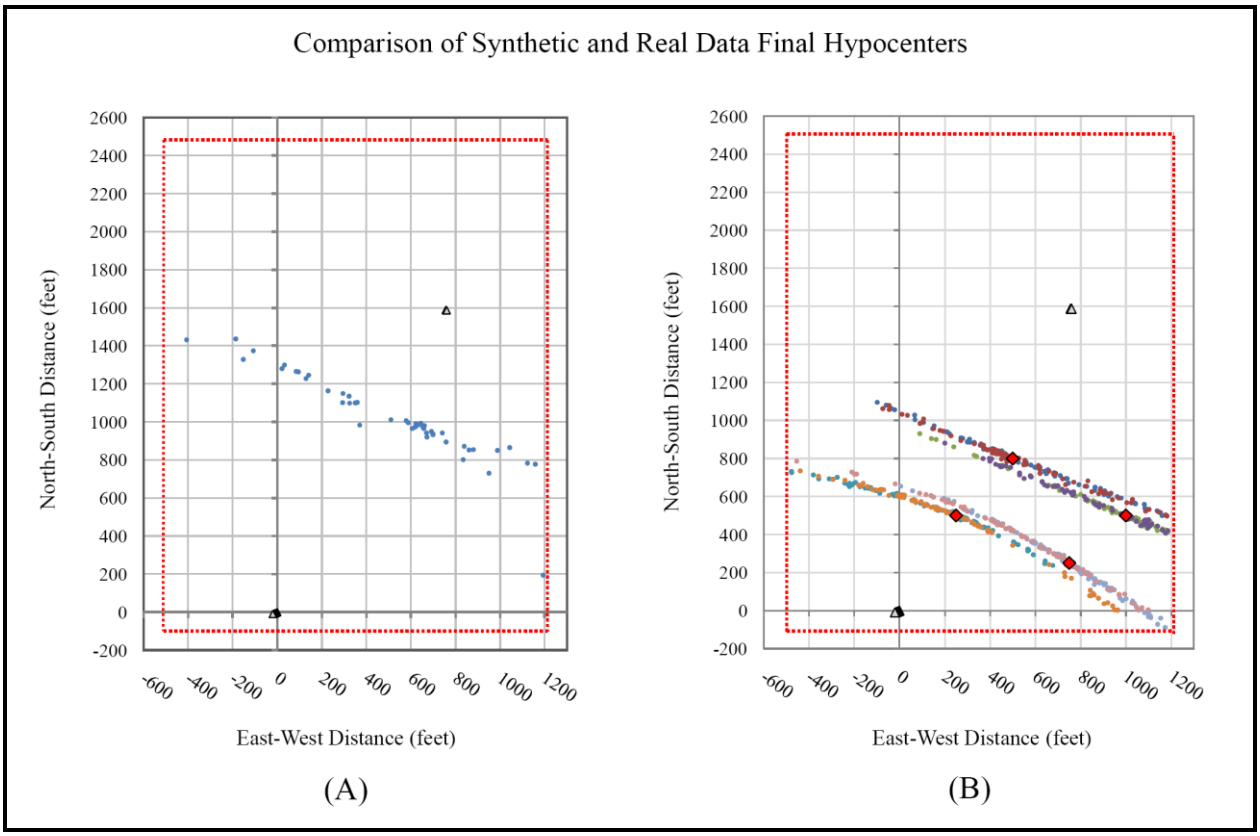

Figure 8.8: Map view comparison of final hypocenters for real data test B-quality picks (A) and synthetic data test with added noise (B). Both show location bias in the direction perpendicular to the between-well line and both extend for similar distances (~2000 feet) along that line. Although the synthetic result appears to model the real data result, the geometric scatter observed for the real data could indicate fractures oriented in the same direction.

			Lowery #3 Well		Lowery #2-26 Well	
			P wave	S wave	P wave	S wave
Quality Category	A	**Total-A**	**55**	**128**	**114**	**80**
		stage 3	12	81	77	49
		stage 4	3	21	14	28
		stage 5	40	26	23	3
	B	**Total-B**	**32**	**198**	**202**	**201**
		stage 3	20	140	147	145
		stage 4	11	45	46	43
		stage 5	1	13	9	13
	C	**Total-C**	**35**	**73**	**82**	**117**
		stage 3	19	55	51	82
		stage 4	16	15	21	10
		stage 5	0	3	10	25
	X	**Total-X**	**277**	**0**	**1**	**1**
		stage 3	225	0	1	0
		stage 4	51	0	0	0
		stage 5	1	0	0	1

Table 8.1: Number of P-wave and S-wave arrivals for receiver arrays at each well assigned to each quality category. Numbers are reported as total arrivals assigned to each category and broken down for each stage of the fracture treatment. Note the large number of X-quality P-wave arrivals for the Lowery #3 well, due to the large distance between the well and earthquakes.

Investigation 5: The Three-well Case with Error

The result of the synthetic test in Investigation 4, where realistic picking error was added to the travel times, showed strong geometric bias on severely mislocated hypocenters. Investigation 3 demonstrated that adding arrival time data from a third observation well could dramatically reduce location errors caused by the lack of geometric constraint in the two-well case. For this investigation, the synthetic test conducted in Investigation 4 was repeated, adding arrival time data from a third vertical observation well to reduce hypocenter location errors caused by the recording geometry.

The three-well geometry used for this test is the same as that used in Test 3 of Investigation 3 (Figure 7.5). New sets of random picking error were generated, using the same normal distribution and standard deviation as Investigation 4, and added to arrival-time picks calculated for all three wells.

Figures 9.1, 9.2, and 9.3 show the final hypocenters, compared to those for the two-well case in Investigation 4. As expected, location errors are significantly reduced by adding arrival-time data from the third well. The average location error is 28.3 feet, nearly an order of magnitude less than the average error for the two-well case in Investigation 4. The average horizontal errors are on the order of one grid cell. The average depth error is more than double the horizontal errors and increases for hypocenters below the depth range of the receivers. This observation is consistent with results using error-free data and three wells, described in Test 3 of Investigation 3.

The result of Investigation 5 demonstrates the potential of improved recording geometry to reduce location errors on real data and provide reasonable hypocenter locations.

Figures

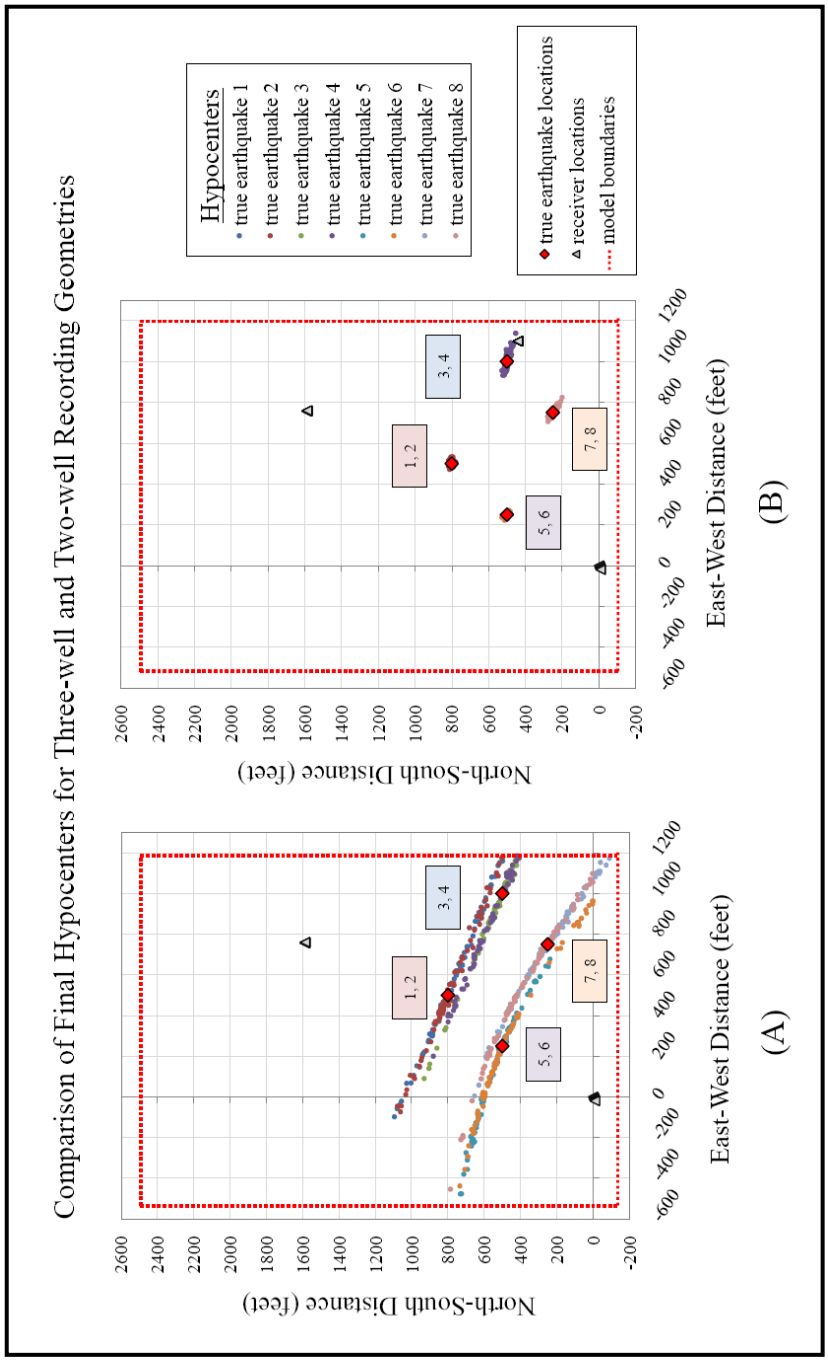

Figure 9.1: Map view comparison of final hypocenters for noisy synthetic data from the two-well case (A) and three-well case (B). Hypocenters for the same true earthquake location are displayed as points of the same color. True earthquake locations are represented by red diamonds; for spatial coordinates [X, Y, Z] of true earthquake locations, refer to Figure 6.4. Receiver stations are represented by gray triangles. Average horizontal location errors reduce to less than a grid cell with the addition of arrival-time data from the third well.

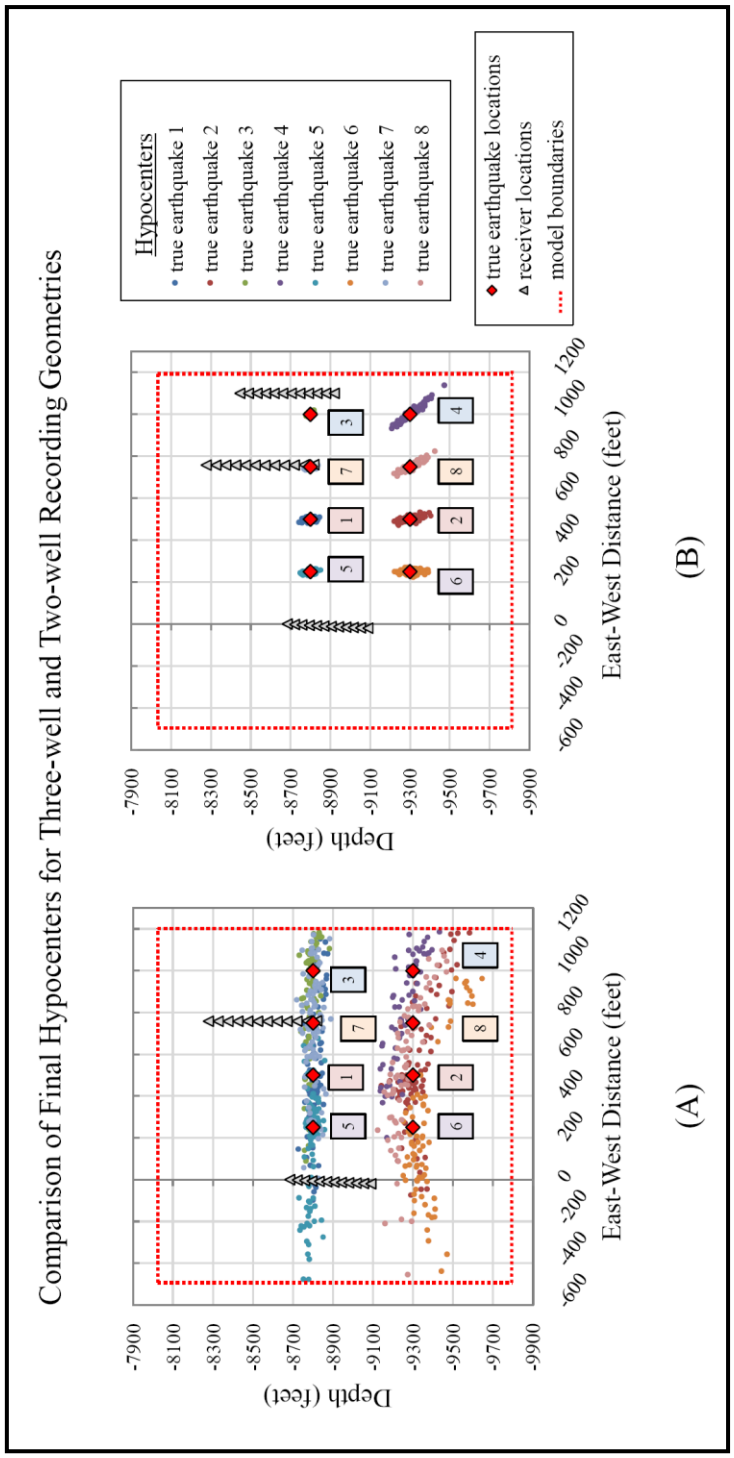

Figure 9.2: East-West cross section comparison of final hypocenters for noisy synthetic data from the two-well case (A) and three-well case (B). Hypocenters for the same true earthquake location are displayed as points of the same color. True earthquake locations are represented by red diamonds; for spatial coordinates [X, Y, Z] of true earthquake locations, refer to Figure 6.4. Receiver stations are represented by gray triangles. For the three-well case, depth errors are significantly larger on earthquakes located below the depth range of receivers. This was also observed in results using entirely error-free data in Test 3 of Investigation 3.

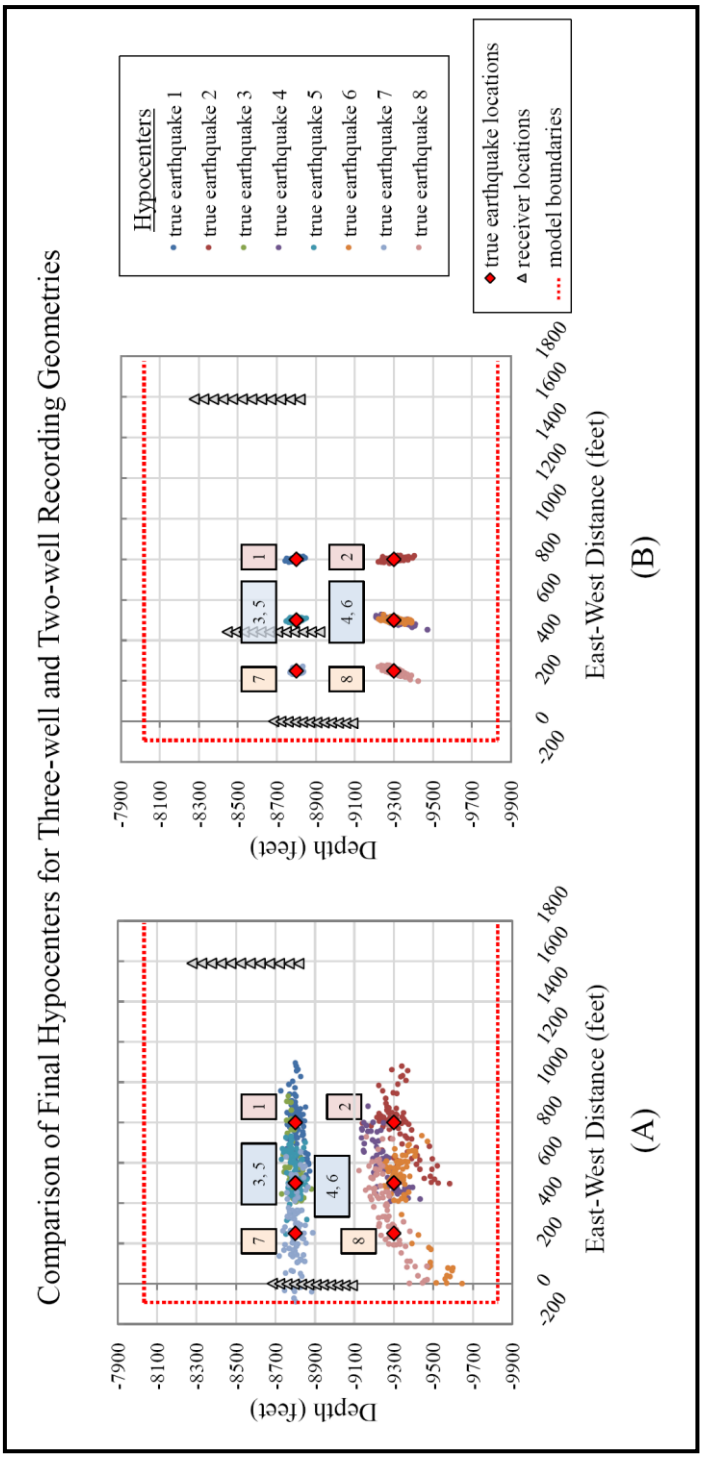

Figure 9.3: North-South cross section comparison of final hypocenters for noisy synthetic data from the two-well case (A) and three-well case (B). Hypocenters for the same true earthquake location are displayed as points of the same color. True earthquake locations are represented by red diamonds; for spatial coordinates [X, Y, Z] of true earthquake locations, refer to Figure 6.4. Receiver stations are represented by gray triangles. For the three-well case, depth errors are significantly larger on earthquakes located below the depth range of receivers. This was also observed in results using entirely error-free data in Test 3 of Investigation 3.

Conclusions

This project was motivated by the potential to improve the characterization of hydro-fracture treated reservoirs using event data recorded simultaneously at two observation wells and a joint hypocenter-velocity tomography algorithm. This analysis could improve the absolute event locations and seismic velocity model obtained with a traditional, single-well data set. The two-well real data set obtained for this purpose exhibited low signal relative to noise. This poor signal, combined with the relatively large distances of the wells from the treatment, meant many of the small-magnitude events could not be detected at both wells. The small amplitude of P-wave arrivals made them especially difficult to pick, resulting in a plan for S-wave-only tomography. During the initial attempt at tomography, hypocenters exhibited anomalous relocation behavior and systematic bias in the direction perpendicular to the line between wells. The focus of the project was redirected to explore the cause of the errors observed on hypocenter relocations.

Tests using the real and representative synthetic data show that the large hypocenter location errors are caused mostly by inadequate recording geometry combined with arrival time noise. Two wells do not surround the earthquake for proper horizontal triangulation of hypocenters, which causes severe bias in the direction perpendicular to the between-well line. This effect is magnified by typical errors that exist on the data, such as arrival time picking errors, and uncertain velocity structure.

One way to attain more accurate locations and potentially perform joint hypocenter-velocity tomography is to change the recording geometry to offer more horizontal constraint, as seen in the synthetic tests that added a third well. For error-free input data, location errors

averaged less than a foot in any direction, and for data with realistic picking error, location errors averaged an order of magnitude less than with only two wells.

Another way to improve constraint and location accuracy is to incorporate both P-wave and S-wave arrival time data simultaneously in the inversion, as is normal for earthquake tomography. Standard single-well surveys use P- and S-wave data to constrain the distance to and depth of an event. If two vertical observation wells were close enough to the earthquakes to record both P- and S-wave arrivals, it is likely that this recording geometry would be sufficient for accurate hypocenter locations in many situations. Three-component particle motion would still be required to determine which of two minima was the true earthquake location. Where only P-wave or S-wave data can be used, adequate constraint requires more than two wells.

To realize the potential of multi-well surveys, the recording geometry must be close enough to events to detect both P- and S-wave arrivals and must provide horizontal location constraint sufficient to overcome the two-minima problem observed in the case of two vertical wells. Location constraint can be improved by reorienting wells or adding wells at new locations. Improvements in reservoir characterization and, ultimately, production are possible by improving the recording geometry, but these benefits must be weighed against the cost and availability of a particular well configuration.

Synthetic test results simulate best-case scenarios and can be a powerful tool for optimizing survey design. Simulating results in advance of drilling and receiver deployment can help determine the best recording geometry to use for the resources available and can provide estimates of minimum error to expect on hypocenter locations.

References

Cited

Beale, J.N., 2004, "Local Earthquake Tomography at Mount Pinatubo, Philippines." Thesis. Virginia Polytechnic Institute and State University.

Boyd, D.T., 2005, Oklahoma Oil and Gas Productions: Its Components and Long-Term Outlook, *Oklahoma Geology Notes*, v. 65, no. 1, pp. 4-23.

Byrnes, A.P. and G. Lawyer, 1999, Burial, Maturation, and Petroleum Generation History of the Arkoma Basin and Ouachita Foldbelt, Oklahoma and Arkansas, *Natural Resources Research*, v. 8, no. 1, pp. 3.-26.

DeCelles, P.G. and K.A. Giles, 1996, Foreland Basin Systems, *Basin Research*, v. 8, pp. 105-123.

Giardini, D., 1992, Lateral Heterogeneity and Earthquake Location, *Physics of the Earth and Planetary Interiors*, v. 75, p.198.

Heran, W.D., Green, G.N., and D.B. Stoeser, 2003. Image. A Digital Geologic Map Database for the State of Oklahoma, *United States Geological Survey*, Open-File Report 03-247. <http://pubs.usgs.gov/of/2003/ofr-03-247>.

Hole, J.A., et al., 2000, Three-dimensional seismic velocity structure of the San Francisco Bay area, *Journal of Geophysical Research*, v. 105, no. B6, p. 13859-13874

Hole, J.A. and B.C. Zelt, 1995, 3-D Finite-difference Reflection Traveltimes, *Geophysical Journal International*, v. 121, pp. 427-434.

Hole, J.A., 1992, Nonlinear High-resolution Three-dimensional Seismic Travel Time Tomography, *Journal of Geophysical Research*, v. 97, no. B5, pp. 6553-6562.

Houseknecht, D.W. and T.A. McGilvery, 1991, Red-Oak Gas-field, Arkoma Basin, OK, *Association of American Petroleum Geologists Bulletin*, v. 75, no. 3, p. 597.

McGilvery, T.A. and D.W. Houseknecht, 2000, Depositional Systems and Diagenesis of Slope and Basin Facies, Atoka Formation, Arkoma Basin, *Oklahoma Geological Survey*, Report: 103, pp. 129-140.

Perry, Jr., W.J., 1995, Arkoma Basin Province (062), *in* Gautier, D. L., Dolton, G.L., Takahashi, K.I., and Varnes, K.L., eds., 1995 National Assessment of United States Oil and Gas Resources--Results, Methodology, and Supporting Data, *United States Geological Survey*, Digital Data Series DDS-30, Release 2, one CD-ROM.

Phillips, W.S. and M.C. Fehler, 1991, Traveltime Tomography: A Comparison of Popular Methods, *Geophysics*, v. 56, no. 10, pp. 1639-1649.

FracSeis Microseismic Fracture Mapping. 2007. Image. Pinnacle Technologies, Inc. <http://www.pinntech.com/microseismic.html>.

Rutledge, J.T., Phillips, W.S., and M.J. Mayerhofer, 2004, Faulting Induced by Forced Fluid Injection and Fluid Flow Forced by Faulting: An Interpretation of Hydraulic-Fracture Microseismicity, Carthage Cotton Valley Gas Field, Texas, *Bulletin of the Seismological Society of America*, v. 94, no. 5, pp. 1817-1830

Schwab, F.L., 1985, Characteristics of Foreland Basin Fill, Abstracts *with Programs—Geological Society of America*, v. 17, no. 7, p. 711.

Vidale, J.E., 1990, Finite-difference Calculation of Traveltimes in Three Dimensions, *Geophysics*, v. 55, no. 5, pp. 521-526.

Whitaker, A.E. and T. Engelder, 2006, Plate-scale Stress Fields Driving the Tectonic Evolution of the Central Ouachita Salient, Oklahoma and Arkansas, *Geological Society of America Bulletin*, v. 118, no. 5/6, pp. 710-723.

Consulted

Bailey, J.R. and W.A. Sorem, 2005, Logging Tool Enables Fracture Characterization for Enhanced Field Recovery, *Society of Petroleum Engineers*, SPE 95909.

Benz, H.M., et al., 1996, Three-dimensional P and S wave Velocity Structure of Redoubt Volcano, Alaska, *Journal of Geophysical Research*, v. 101, no. B4, pp. 8111-8128.

Brancato, A., et al., 2009, Determination of Seismogenic Structures in Southeastern Sicily (Italy) by High-Precision Relative Relocation of Microearthquakes, *Bulletin of the Seismological Society of America*, v. 99, no. 3, pp. 1921-1936.

Diehl, T., et al., 2009, Automatic S-Wave Picker for Local Earthquake Tomography, *Bulletin of the Seismological Society of America*, v.99, no. 3, pp. 1906-1920.

Fukuyama, E., et al., 2003, Detailed Fault Structure of the 2000 Western Tottori, Japan, Earthquake Sequence, *Bulletin of the Seismological Society of America*, v. 93, no. 4, pp. 1468-1478.

Koulakov, I., 2009, LOTOS Code for Local Earthquake Tomographic Inversion: Benchmarks for Testing Tomographic Algorithms, *Bulletin of the Seismological Society of America*, v. 99, no. 1, pp. 194-214.

Mahrer, K.D., Aud, W.W., and J.T. Hansen, 1996, Far-field Hydraulic Fracture Geometry: A Changing Paradigm, *Society of Petroleum Engineers*, SPE 36441.

Maxwell, S.C., et al., 2002, Microseismic Imaging of Hydraulic Fracture Complexity in the Barnett Shale, *Society of Petroleum Engineers*, SPE 77440.

Pesicek, J.D., et al., 2008, Three-dimensional P-wave Velocity Structure and Precise Earthquake Relocation at Great Sitkin Volcano, Alaska, *Bulletin of the Seismological Society of America*, v. 98, no. 5, pp. 2428-2448.

Richards, P.G., et al., 2006, The Applicability of Modern Methods of Earthquake Location, *Pure and Applied Geophysics*, v. 163, pp. 351-372.

Satriano, C., Zollo, A., and C. Rowe, 2008, Iterative Tomographic Analysis Based on Automatic Refined Picking, *Geophysical Prospecting*, v. 56, pp. 467-475.

Tura, M.A.C., Greaves, R.J., and W.B. Beydouns, 1994, Crosswell Seismic Reflection/Diffraction Tomography: A Reservoir Characterization Application, *Geophysics*, v. 59, no. 3, pp. 351-361.

Waldhauser, F. and W.L. Ellsworth, 2000, A Double-difference Earthquake Location Algorithm: Method and Application to the Northern Hayward Fault, California, *Bulletin of the Seismological Society of America*, v. 90, no. 6, pp. 1353-1368.

Zelt, B.C., et al., 1996, Inversion of Three-dimensional Wide-angle Seismic Data from the Southwestern Canadian Cordillera, *Journal of Geophysical Research*, v. 101, no. B4, pp. 8503-8529.

Zhang, H. and C. Thurber, 2006, Development and Applications of Double-difference Seismic Tomography, *Pure and Applied Geophysics*, v. 163, pp. 373-403.

Zhao, A. and Z. Ding, 2009, Earthquake Location in Transversely Isotropic Media with a Tilted Symmetry Axis, *Journal of Seismology*, v. 13, pp. 301-311.